Controlling the Size of Molecular Copper Clusters Supported by a Multinucleating Macrocycle

*Qiuran Wang, Ryan P. Murphy, Michael R. Gau, Patrick J. Carroll, Neil C. Tomson**

Department of Chemistry, University of Pennsylvania, 231 South 34th Street, Philadelphia, PA, 19104, United States

ABSTRACT The use of a non-rigid, pyridyldialdimine-derived macrocyclic ligand (^{3}PDAI$_2$) enabled the synthesis of well-defined mono-, di-, tri-, and tetra-nuclear Cu(I) complexes in good yields through rational synthetic means. Starting from mono- and di-argentous ^{3}PDAI$_2$ complexes, transmetallation to Cu(I) proceeded smoothly with formation of AgX (X = Cl, I) salts to generate mono-, di-, and tri-nuclear copper complexes. Monodentate supporting ligands (MeCN, xylNC, PMe$_3$, PPh$_3$) were found to either transmetallate with or bind various di- and tri-nuclear clusters. The solution-phase dynamic behaviors of these species were studied through NMR spectroscopic investigations, and an in-depth study of the trinuclear systems revealed a rate dependence on the identity of the supporting ligand, indicating that ligand dissociation reactions were involved in the dynamic exchange processes. Synthetic

investigations further found methods for the purposeful interconversion between the di- and tri-nuclear systems as well as the synthesis of a pseudo-tetrahedral tetracopper complex with two μ-Ph supporting ligands.

Introduction

The rational synthesis of well-defined cluster complexes is a subject of intense investigation in the field. Atomically precise clusters are being used to understand the mechanisms of nanoparticle formation,[1] to synthesize large clusters with unique properties,[2] and to model the active sites of various metalloenzymes and solid-state surfaces.[3-9] The synthesis of atomically precise Cu(I) cluster complexes is an important subset of this field.[10-12] These systems can display interesting photophysical[13-15] and chemical properties,[16-26] while their metallophilic Cu(I)-Cu(I) interactions offer opportunities to advance bonding theories and computational chemistry.[27-30]

A key challenge in the study of Cu(I) clusters is the ability of these systems to redistribute their metal ions.[31-37] These facile redistribution processes typically lead to the isolation of thermodynamically preferred cluster sizes.[38-40] Given the importance of cluster size and geometry to the properties they manifest,[11, 41-48] it would be advantageous to develop strategies for mitigating the ability of multicopper assemblies to redistribute while enforcing atypical geometries. We envisioned the use of multitopic and multinucleating ligands for kinetically stabilizing Cu(I) clusters through control over the cluster's coordination sphere,[6, 26, 49, 50] but ligand design for multinuclear systems

is in its infancy.[51] Recent work with Cu(I) complexes has highlighted the advantages offered by dinucleating and trinucleating ligand scaffolds,[6, 24, 26, 50, 52-60] suggesting that further ligand design may offer a path forward for the modular construction of low-nuclearity Cu(I) clusters.

We have shown the ability of a class of pyridyldiimine-derived macrocyclic ligands to support [Fe_2], [Co_2], [Ni_2], and [Cu_2] cluster cores.[8, 61-68] These ligands combine two pyridyldiimine moieties through flexible aliphatic linkers at the imine nitrogens to create the diketimine-based ^{3}PDI$_2$ ligand framework. We recently reported the ability of a related dialdimine-based ^{3}PDAI$_2$ ligand system to support mono- and di-argentous complexes.[69] Given the smaller atomic radius of Cu (1.173 Å) compared to Ag (1.339 Å),[70] we reasoned that the cavity formed by the ^{3}PDAI$_2$ ligand may accommodate Cu(I) clusters with nuclearities larger than two, while offering improved control over the coordination environment about the Cu cluster compared to systems with unsupported Cu–Cu interactions. As will be shown in this contribution, the ^{3}PDAI$_2$-supported Ag(I) complexes can be used as templates for the formation of Cu(I) complexes *via* the precipitation of Ag(I) salts.[14] The resulting mono- and di-cuprous complexes can then be used for generating well-defined examples of tri- and tetra-cuprous cluster complexes. This system is further shown to allow for facile interconversion between di- and tri-nuclear species through rational addition and removal of Cu(I) ions. The combination of this synthetic chemistry with the spectroscopic studies of their

behaviors in solution reveals the ability of the ^{3}PDAI$_2$ macrocycle to kinetically stabilize clusters of various sizes with respect to redistribution processes.

Results and Discussion

Synthesis of a Mononuclear Copper Complex

Treatment of a THF solution of [(^{3}PDAI$_2$)Ag][BPh$_4$] (**[Ag]$^+$**)[69] with 1.0 equiv. of CuI resulted in an immediate color change from pale gold to dark red-purple with concomitant formation of a pale yellow precipitate, presumably AgI. Following crystallization, dark red crystals were obtained and identified by single crystal X-ray diffractometry to be the monocopper complex [(^{3}PDAI$_2$)Cu][BPh$_4$] (**[Cu]$^+$**, Scheme 1, Figure 1a).

Scheme 1. Transmetallation to form **[Cu]$^+$**.

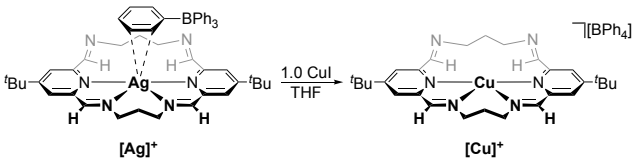

The metal center in **[Cu]$^+$** adopts a distorted tetrahedral geometry ($\Sigma\angle$N–Cu–N = 382.0°, τ_4 = 0.98,[71] Table 1) and unlike the starting material,[69] the [BPh$_4$]$^-$ anion is outer-sphere, as indicated by the long distance between the copper center and its closest C=C bond on [BPh$_4$]$^-$ (d(Cu···Ct$_{cc}$) = 4.030 Å). The cuprous ion, however, retains the coordination environment of Ag$^+$ within the macrocycle; both are coordinated by two

pyridyl nitrogen atoms (avg. d(Cu–N_{pyr}) = 2.047 Å) and two propylene-linked nitrogen atoms (avg. d(Cu–N_{ald}) = 2.095 Å), with the Cu–N distances *ca.* 0.3 Å shorter. The difference in the first coordination spheres of the metal centers is likely the result of the smaller single-bond covalent radius of Cu (1.173 Å *vs.* 1.339 Å of Ag).[70] The lone pairs on the unbound N_{ald} atoms in **[Cu]**$^+$ point away from the metal center to yield a conformation similar to that of **[Ag]**$^+$. The amount of electron density delocalized into the π* manifold of PD(A)I-based ligands has been parameterized through a Δ parameter.[61, 72] The Δ value for **[Cu]**$^+$ of 0.168 Å is indicative of a modest increase in ligand-based electron density compared with **[Ag]**$^+$ (Δ = 0.178 Å), though both are in the range of Δ values that are best associated with $(^3PDAI_2)^0$ oxidation states. The ^{1}H NMR spectrum of **[Cu]**$^+$ in THF-d_8 indicates that the compound exhibits D_{2h} symmetry in solution at room temperature on the NMR timescale, as indicated by the 8:4 pattern of the ^{1}H NMR signals from the $(CH_2)_3$ linker protons (see Supporting Information, Figure S1). These data are consistent with the symmetry observed for other mononuclear complexes bound by this ligand and indicate that a dynamic rearrangement process is occurring in solution.[69, 73] However, given the lability of ligand binding to Cu(I) and the propensity of Cu(I) ions to associate into clusters, the rearrangement process may involve the dissociation and association of Cu(I) ions. We thus next sought the synthesis of multinuclear Cu(I) systems in an effort to evaluate the suitability of the $^3PDAI_2$ macrocycle for kinetically stabilizing multinuclear Cu(I) systems against redistribution of their metal ions.

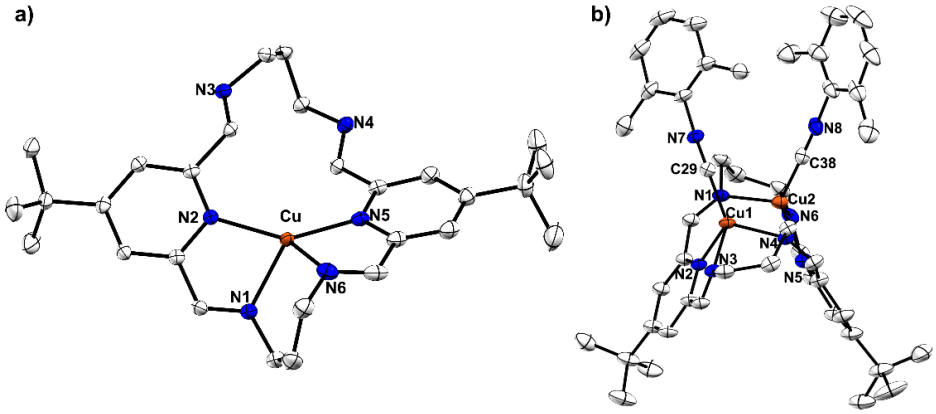

Figure 1. Crystal structures of the cationic portion of a) **[Cu]**$^{+}$ and b) **[Cu$_2$(CNxyl)$_2$]**$^{2+}$ with thermal ellipsoids at the 50% probability level. Hydrogen atoms were omitted for clarity.

Table 1. Averaged crystallographic metrics of **[Cu]**$^{+}$ and **[Cu$_2$(CNxyl)$_2$]**$^{2+}$.

	[Cu]$^{+}$	**[Cu$_2$(CNxyl)$_2$]**$^{2+}$
d(Cu···Cu) / Å	-	2.9905(5)
d(Cu–C) / Å	-	1.856
d(Cu–N$_{py}$) / Å	2.0473	2.075
d(Cu–N$_{ald}$) / Å	2.0946	2.084
d(N$_{py}$-C$_{ipso}$) / Å	1.354	1.351
d(C$_{ipso}$-C$_{ald}$) / Å	1.479	1.476
d(C$_{ald}$-N$_{ald}$) / Å	1.270	1.274
Δ_{expt} / Å	0.168	0.164
FSR	-	1.27
τ_4	0.98	0.79

Syntheses of Multinuclear Copper Complexes

The success of using **[Ag]**$^{+}$ as the template for the monocopper complex **[Cu]**$^{+}$ prompted our investigation into the use of the previously reported diargentous complexes [(^{3}PDAI$_{2}$)Ag(CNxyl)$_{2}$][OTf]$_{2}$ (**[Ag$_{2}$(CNxyl)$_{2}$]$^{2+}$**) and [(^{3}PDAI$_{2}$)Ag(PPh$_{3}$)$_{2}$][OTf]$_{2}$ (**[Ag$_{2}$(PPh$_{3}$)$_{2}$]$^{2+}$**) to synthesize the corresponding dicuprous complexes. The addition of 2.0 equiv of CuI to a stirring solution of **[Ag$_{2}$(CNxyl)$_{2}$]$^{2+}$** in THF led to an immediate color change from pale yellow to a dark orange-red with the formation of a yellow precipitate. Following work-up and purification, red crystals of [(^{3}PDAI$_{2}$)Cu(CNxyl)$_{2}$][OTf]$_{2}$ (**[Cu$_{2}$(CNxyl)$_{2}$]$^{2+}$**, Scheme 2) were isolated with a yield of 78 %.

Scheme 2. Syntheses of **[Cu$_{2}$(CNxyl)$_{2}$]$^{2+}$**.

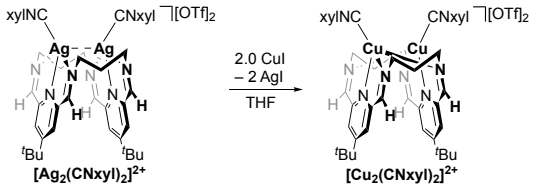

The molecular structure of **[Cu$_{2}$(CNxyl)$_{2}$]$^{2+}$** was determined crystallographically (Figure 1b). Two molecules of **[Cu$_{2}$(CNxyl)$_{2}$]$^{2+}$** are present in the asymmetric unit. One of the molecules, which is well defined, presented a shorter Cu–Cu distance (2.9905(5) Å) and a larger Δ value (0.164 Å), while the other molecule, which is disordered (see Supplementary Information for more details), exhibits an elongated Cu–Cu distance (3.148(4) Å) and a smaller Δ value (0.153 Å). Despite these apparent differences, NMR

spectra of **[Cu$_2$(CNxyl)$_2$]$^{2+}$** show the presence of only one species, supporting the notion that these variances are a result of crystal packing. The following discussion will thus be based on the structure of the more well-defined molecule in the asymmetric unit. While **[Cu(CNxyl)$_2$]$^{2+}$** and **[Ag$_2$(CNxyl)$_2$]$^{2+}$** are isoelectronic to one another, the coordination environment about the dinuclear core in **[Cu$_2$(CNxyl)$_2$]$^{2+}$** is distinct. Each Ag center in **[Ag$_2$(CNxyl)$_2$]$^{2+}$** is held within one PDAI unit,[69] but each Cu center in **[Cu$_2$(CNxyl)$_2$]$^{2+}$** is coordinated to two N_{ald} atoms connected by the same $(CH_2)_3$ linker and one N_{py} atom. As a result, the Cu centers each adopt a distorted tetrahedral geometry, evident from both the large avg. τ_4 value of 0.79 (Table 1) and the sum of bond angles around the Cu atom (avg. Σ∠L–Cu–L = 399.7°, L = N, C). The distance between the two Cu centers (2.9905(5) Å) is long and larger than the sum of the van der Waals radius of Cu.[74] The long intermetallic distance, combined with the large formal shortness ratio (FSR)[75] of 1.27, is indicative of minimal Cu···Cu interactions in this complex. The Δ value of the ^{3}PDAI$_2$ ligand of 0.164 Å is indicative of a neutral ligand with slight electron density delocalization over the PDAI moieties.[61] The room temperature ^{1}H NMR spectrum of **[Cu$_2$(CNxyl)$_2$]$^{2+}$** is consistent with a C_{2v}-symmetric geometry, as determined by the 4:4:2:2 grouping of the proton signals associated with the $(CH_2)_3$ linkers (see Supporting Information, Figure S7), suggesting that **[Cu$_2$(CNxyl)$_2$]$^{2+}$** retains the folded ligand geometry observed crystallographically when placed in solution but that the Cu coordination geometries are dynamic within the ligand binding pocket at room temperature on the ^{1}H and ^{13}C NMR timescales.

Interestingly, treatment of **[Ag$_2$(PPh$_3$)$_2$]$^{2+}$** with 2.0 equiv. of CuCl did not lead to the formation of a dicuprous PPh$_3$ complex; instead, a tricuprous species, [(^{3}PDAI$_2$)Cu$_3$Cl(PPh$_3$)$_2$][OTf]$_2$ (**[Cu$_3$Cl(PPh$_3$)$_2$]$^{2+}$**) was isolated. **[Cu$_3$Cl(PPh$_3$)$_2$]$^{2+}$** was also formed in a yield of 79 % when 3.0 equiv. of CuCl were used. Subsequent investigations found that treatment of a slurry of **[Ag$_2$(NCMe)$_2$]$^{2+}$** in THF with 2.0 equiv. of an L-type ligand (L = PPh$_3$, PMe$_3$, xylNC), followed by 3.0 equiv. of CuCl afforded a series of isomorphic tricopper complexes, [(^{3}PDAI$_2$)Cu$_3$ClL$_2$][OTf]$_2$ (L = PPh$_3$ (**[Cu$_3$Cl(PPh$_3$)$_2$]$^{2+}$**), PMe$_3$ (**[Cu$_3$Cl(PMe$_3$)$_2$]$^{2+}$**), and CNxyl (**[Cu$_3$Cl(CNxyl)$_2$]$^{2+}$**)). Additionally, treatment of **[Ag$_2$(NCMe)]$^{2+}$** with 3.0 equiv of CuCl in acetonitrile led to the formation of **[Cu$_3$Cl(NCMe)$_2$][OTf]$_2$** (Scheme 3).

Scheme 3. Syntheses of **[Cu$_3$Cl(L)$_2$]$^{2+}$**.

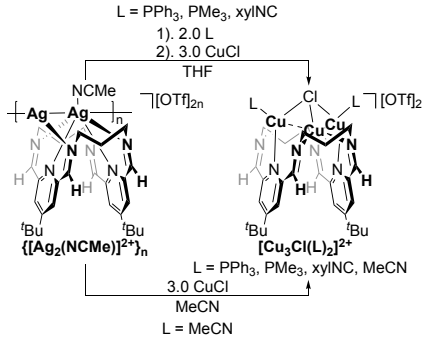

The **[Cu$_3$Cl(L)$_2$]$^{2+}$** complexes are isostructural, and all include a folded ^{3}PDAI$_2$ ligand (Figure 2). The Δ values of *ca.* 0.165 Å indicate that the ^{3}PDAI$_2$ ligands in these complexes are neutral (Table 2). Each copper center is coordinated by two macrocycle-based nitrogen atoms and a single μ_3-Cl atom, with Cu1 and Cu2 each ligating a Lewis base. Cu1 and Cu3 are each coordinated by one N$_{py}$ and an adjacent N$_{im}$, while Cu2 is

bound by two N_{im} donors linked by a propylene tether. Cu1 and Cu3 both adopt a tetrahedral geometry, but the geometry of Cu2 is close to trigonal planar, as indicated by the sum of bond angles around it (Σ∠E–Cu2–E = *ca.* 355°, E = N, Cl). Within the $[Cu_3Cl]^{2+}$ cores, the chlorides lie above the $[Cu_3]$ planes and are not equivalently coordinated to the three copper centers, as indicated by the shorter Cu2–Cl bond lengths (*ca.* 2.2 Å) compared to the other two within each complex (> 2.36 Å).

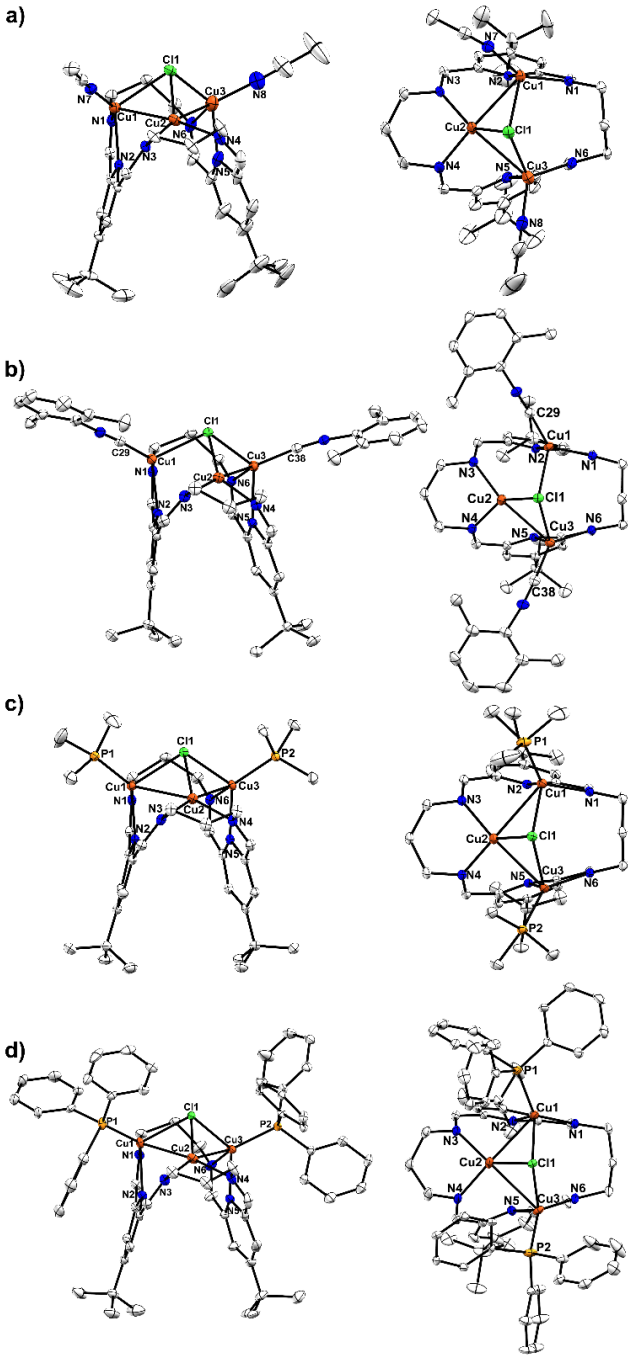

Figure 2. Crystal structures of a) **[Cu$_3$Cl(NCMe)$_2$]$^{2+}$**, b) **[Cu$_3$Cl(CNxyl)$_2$]$^{2+}$**, c) **[Cu$_3$Cl(PMe$_3$)$_2$]$^{2+}$** and d) **[Cu$_3$Cl(PPh$_3$)$_2$]$^{2+}$** with thermal ellipsoids at the 50% probability level. Left: side view; right: top view. Hydrogen atoms and counter ions were omitted for clarity.

Overall, the symmetry of each complex in this series can be considered *pseudo-*C_s, with a mirror plane containing Cu2 and relating Cu1 to Cu3. Further, the ∠Cu1–Cu2–Cu3 angles of *ca.* 90° place the three coppers in each complex in an isosceles right triangle geometry. This geometry is extremely rare in molecular complexes.[76] Ligand-supported $[Cu_3Cl]$ cores are typically (*pseudo-*)C_{3v}-symmetric, as indicated by their nearly identical Cu–Cu–Cu bond angles,[6, 77-80] and among molecular complexes that consist of a $[Cu_3Cl]$ scaffold with a right-angled $[Cu_3]$ fragment, the $[Cu_3Cl]$ cores are either planar[81] or part of a larger $[Cu_xCl_y]$ cluster.[82-86] A $[Cu_3Cl]$ scaffold reported in 2004 by Sutter, Chaudhury, and coworkers is most similar to those reported here but is composed of Cu(II) centers and exhibits significantly longer Cu···Cu (*ca.* 3.2 Å to *ca.* 4.8 Å) and Cu–Cl distances (> 2.6 Å), making it distinct from the $[Cu_3Cl]^{2+}$ core in **$[Cu_3Cl(L)_2]^{2+}$**.[87] Notably, the unique triangular shape of the $[Cu_3Cl]^{2+}$ cluster cores in **$[Cu_3Cl(L)_2]^{2+}$** is reminiscent of the alignment of the three Cu centers in the fully reduced state of the ascorbate oxidase class of multicopper oxidase metalloenzymes.[88] The potential for studying of relationship of **$[Cu_3Cl(L)_2]^{2+}$** to the active sites in multicopper oxidases prompted investigations into whether or not the geometries of the $[Cu_3Cl]^{2+}$ cores persisted in solution.

Table 2. Averaged crystallographic metrics of **$[Cu_3Cl(L)_2]^{2+}$** (L = NCMe, CNxyl, PMe_3, PPh_3).

	$[Cu_3Cl(NCMe)_2]^{2+}$	**$[Cu_3Cl(CNxyl)_2]^{2+}$**	**$[Cu_3Cl(PMe_3)_2]^{2+}$**	**$[Cu_3Cl(PPh_3)_2]^{2+}$**

d(Cu1···Cu2) / Å	2.8330(6)	3.0316(2)	2.8288(3)	2.7099(3)
d(Cu2···Cu3) / Å	2.6980(5)	2.7185(3)	2.7230(3)	2.8313(3)
d(Cu1···Cu3) / Å	3.8340(9)	4.0668(5)	4.0242(4)	3.9383(6)
d(Cu–L) / Å	1.912	1.856	2.1865	2.1977
d(Cu–N_{py}) / Å	2.192	2.1795	2.1472	2.1767
d(Cu–N_{ald}) / Å	1.995	2.0070	2.0126	2.0116
d(N_{py}-C_{ipso}) / Å	1.348	1.349	1.348	1.348
d(C_{ipso}-C_{ald}) / Å	1.473	1.477	1.475	1.474
d(C_{ald}-N_{ald}) / Å	1.273	1.274	1.272	1.274
Δ_{expt} / Å	0.163	0.165	0.165	0.163
FSR(Cu1···Cu2)	1.15	1.29	1.21	1.16
FSR(Cu2···Cu3)	1.21	1.16	1.16	1.21
FSR(Cu1···Cu3)	1.63	1.73	1.72	1.68
∠Cu1–Cu2–Cu3 / °	87.730(15)	89.859(9)	92.892(9)	90.561(1)
Σ∠E–Cu2–E[a] / °	352.04	356.48	354.04	354.49
τ_4[a]	0.75	0.78	0.74	0.80

[a] E = N, Cl

[b] value of Cu1 and Cu3

Dynamic Exchange within the Tricopper Clusters

The **[Cu$_3$Cl(L)$_2$]$^{2+}$** complexes display *pseudo-C$_s$* symmetry in the solid state, but their NMR spectra in CD_3CN are of higher symmetry at room temperature. Interestingly, the symmetries of these complexes in solution depend on the identity of the L-type ligand bound to the Cu1 and Cu3 atoms (Figure 3). The room temperature ^{1}H NMR spectrum

of [**$Cu_3Cl(NCMe)_2$**]$^{2+}$ revealed a D_{2h}-symmetric complex, as indicated by the 8:4 pattern of well-defined signals from the $(CH_2)_3$ protons. The ^{1}H NMR spectrum of [**$Cu_3Cl(CNxyl)_2$**]$^{2+}$, however, reveals a modestly broadened signal integrating to 8H for the hydrogens α to the aldimino nitrogens (α-CH_2) and broad, low-intensity signals for the linker hydrogens β to the aldimino nitrogens (β-CH_2). These features indicate that the coalescence temperatures of the propylene linker protons are close to room temperature and that the exchange process responsible for the equilibration of the linker protons has a larger activation energy for L = CNxyl. The activation energy appears to increase again for L = PMe_3; the ^{1}H NMR resonances for the β-CH_2 protons of [**$Cu_3Cl(PMe_3)_2$**]$^{2+}$ appear as two well-defined, albeit broad, signals. Finally, the PPh_3-bound complex [**$Cu_3Cl(PPh_3)_2$**]$^{2+}$ displays the lowest symmetry in CD_3CN at room temperature, as indicated by the 4:4:2:2 pattern of ^{1}H NMR resonances from the $(CH_2)_3$ linker hydrogens. The solution-phase symmetry is still higher than that observed in the crystal structure of this complex – the aldimino hydrogen and pyridyl hydrogen signals for all complexes each appear as singlets that integrate to 4H at *ca.* 8.5 and 7.5 ppm, respectively (Figure 3) – but the activation energy associated with the overall exchange process in solution for [**$Cu_3Cl(PPh_3)_2$**]$^{2+}$ appears to be the highest of the series.

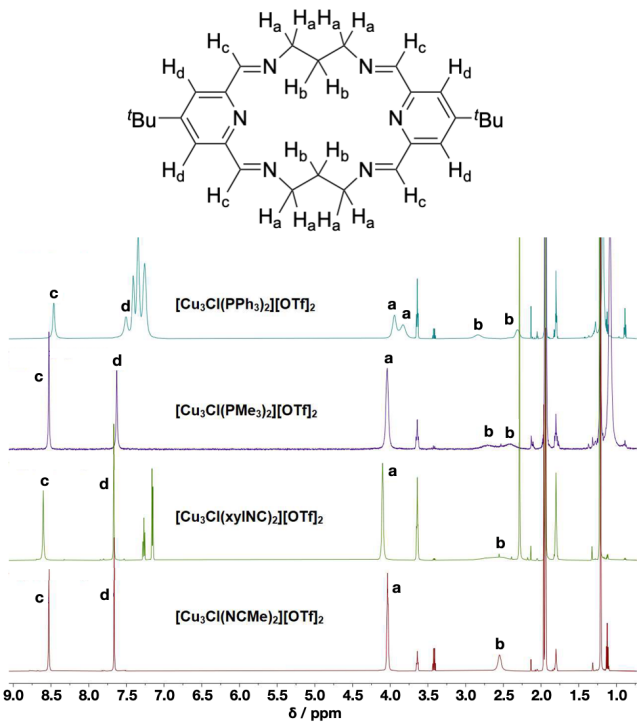

Figure 3. ^{1}H NMR spectra of **[Cu$_3$Cl(L)$_2$]$^{2+}$** in CD_3CN at room temperature. Signals from α-CH_2 are labelled with "a", signals from β-CH_2 groups of the linker are labelled with "b", aldimino hydrogen signals are labelled with "c", and pyr-H signals are labelled with "d".

For the ^{1}H NMR spectroscopic resonances associated with the propylene linker protons of the **[Cu$_3$Cl(L)$_2$]$^{2+}$** complexes to exhibit the averaging observed experimentally, several dynamic exchange processes need to occur in solution (Scheme 4). Coalescence/broadening of the α-CH_2 signals must result from an inversion of the folded geometry of the macrocycle ligand. This process necessitates a net inversion of the orientation of the cone formed by the Cu_3Cl core for the chemical environments of the diastereotopic hydrogens on the $(CH_2)_3$ linker to equilibrate. However, these two

processes by themselves cannot account for the coalescence of the signals from the pyridyl or aldimino hydrogens. Thus, a process that involves the dynamic exchange of the PDAI coordination mode to the $[Cu_3Cl(L)_2]^{2+}$ core is also necessary.

The steric profile of the $[Cu_3Cl(L)_2]^{2+}$ cores are larger than the cavity of the $^3PDAI_2$ ligand, so the partial dissociation of the $[Cu_3Cl(L)_2]^{2+}$ cluster is essential for the ligand conformational exchange to happen (Scheme 4). The observed solution phase symmetry of each **$[Cu_3Cl(L)_2]^{2+}$** complex is dependent on the identity of L (Figure 3), indicating that the dynamic processes discussed above likely involve the dissociation of the L fragments. We further reasoned that the dissociation/re-association of a Cu^+ ion or a CuCl fragment might also be involved in changing both the orientation of the $[Cu_3Cl]^{2+}$ core and the PDAI coordination mode. This latter proposal is supported by the observed C_{2v} solution-phase symmetry of the dicuprous isocyanide species **$[Cu_2(CNxyl)_2]^{2+}$**. However, attempts to bias this proposed equilibrium toward the tricuprous species through addition of $[Cu(MeCN)_4][OTf]$ or CuCl to a CD_3CN solution of **$[Cu_3Cl(PPh_3)_2]^{2+}$** resulted in a *higher* solution-phase symmetry at room temperature (see Supporting Information, Figures S40 and S41). This observation suggests that even higher nuclearity clusters supported by the $^3PDAI_2$ macrocycle may be accessible (see below).

Scheme 4. Proposed dynamic exchange processes that result in higher in-solution symmetry of **$[Cu_3Cl(L)_2]^{2+}$** complexes at room temperature.

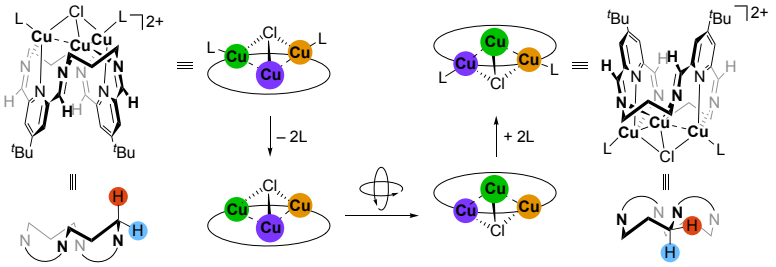

To further probe the dynamic processes in solution, variable-temperature NMR spectroscopic studies on **[Cu$_3$Cl(PPh$_3$)$_2$]$^{2+}$** were carried out. The variable-temperature NMR spectra of **[Cu$_3$Cl(PPh$_3$)$_2$]$^{2+}$** in CD_3CN are shown in Figure 4 and additional data are provided in the Supplementary Information (Figure S42). At temperatures higher than room temperature, the pyr-H signals and aldimino proton signals remain as singlets, and the coalescence of the $(CH_2)_3$ linker proton signals is apparent as the temperature is increased from 298 K. The two α-CH_2 signals merge into one broad singlet between 308 K and 318 K. The signal sharpens as the temperature is increased further. The coalescence of the β-CH_2 signals occurs between 318 K and 328 K. As expected, the behavior of the α/β-CH_2 ^{1}H NMR signals at elevated temperatures repeats in the other **[Cu$_3$Cl(L)$_2$]$^{2+}$** complexes (L = MeCN, xylNC and PMe_3, Figure 5), albeit with different coalescence temperatures. The data for **[Cu$_3$Cl(PPh$_3$)$_2$]$^{2+}$** at 318 K, 328 K and 338 K are qualitatively identical to those observed in the room temperature spectra of, respectively, **[Cu$_3$Cl(PMe$_3$)$_2$]$^{2+}$**, **[Cu$_3$Cl(CNxyl)$_2$]$^{2+}$**, and **[Cu$_3$Cl(NCMe)$_2$]$^{2+}$**. It can thus be concluded that the rates of the overall dynamic exchange process (k_{ex}) of the **[Cu$_3$Cl(L)$_2$]$^{2+}$** complexes follow the trend k_{ex}(L = PPh_3) < k_{ex}(L = PMe_3) < k_{ex}(L = xylNC) < k_{ex}(L = MeCN) in CD_3CN. The dependence of k_{ex} on the identity of L, coupled with

the convergence of the high T spectral pattern for L = PPh_3 (lowest k_{ex}) on the spectral trace observed at room temperature for L = MeCN (fastest k_{ex}), suggests that the slowest dynamic process in solution represents the dissociation of L to transiently form **$[Cu_3Cl]^{2+}$**. This Lewis base-free complex would then undergo additional rapid dynamic exchange processes to generate the observed D_{2h} symmetry.

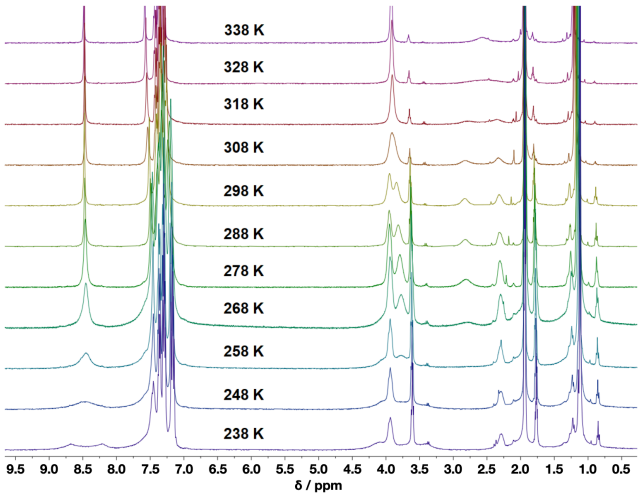

Figure 4. Variable-temperature ^1H NMR spectra of **$[Cu_3Cl(PPh_3)_2]^{2+}$** in CD_3CN in the range of 238 to 338 K. The results of two separate experiments (238 K to 298 K and 308 K to 338K, respectively) were combined.

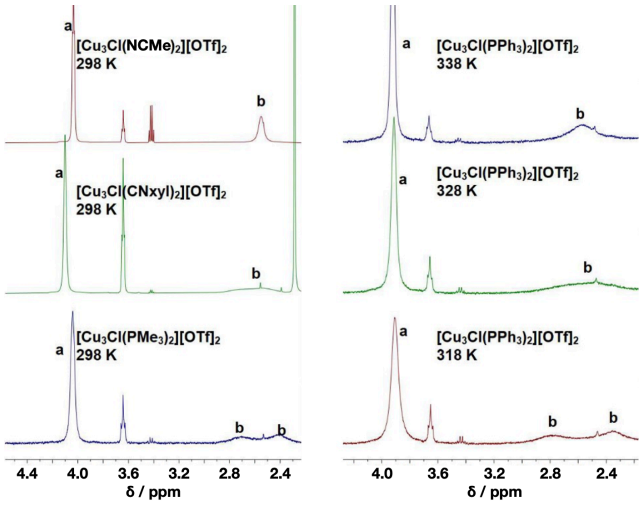

Figure 5. Comparison of the ^{1}H NMR resonances of the protons on the propylene linkers of **[Cu$_3$Cl(L)$_2$]$^{2+}$** (L = MeCN, xylNC, PMe$_3$) in CD$_3$CN at 298 K (left) with the corresponding resonances of **[Cu$_3$Cl(PPh$_3$)$_2$]$^{2+}$** in CD$_3$CN at different temperatures (right). The α-CH$_2$ signals are labelled with "a" and the β-CH$_2$ resonances are labelled with "b".

The ^{1}H NMR spectra of **[Cu$_3$Cl(PPh$_3$)$_2$]$^{2+}$** in CD$_3$CN at temperatures lower than 298 K (Figure 4) revealed the de-coalescence of signals at *ca.* 8.5 ppm (aldimine), *ca.* 3.8 ppm (α-CH$_2$) and *ca.* 2.8 ppm (β-CH$_2$) as the temperature was decreased to 238 K. Unfortunately, these features were not fully resolved before the melting point of CD$_3$CN was reached, making it difficult to extract quantitative information on activation energies. We thus turned to the use of CD$_2$Cl$_2$ as a solvent and were interested to find some disparity in the apparent rates of dynamic exchange in CD$_2$Cl$_2$ compared to those in CD$_3$CN at 298 K, likely due to the involvement of acetonitrile exchange in the dynamic process. The pyr-H and aldimine signals were significantly more

broadened in CD_2Cl_2, but the linker protons exhibited a comparable amount of broadening between the two solvents (see Supporting Information, Figure S43). The pattern and integrations of the signals observed for the α/β-CH_2 linker protons indicate that **[Cu$_3$Cl(PPh$_3$)$_2$]$^{2+}$** exhibits a lower-than-D_{2h} symmetry at 298 K in CD_2Cl_2, but the broadened, weak signals prevent further detailed analysis.

More defined ^{1}H NMR signals were found to evolve as the temperature of the CD_2Cl_2 system was decreased. The ^{1}H NMR spectrum at 213 K contains well-defined signals (Figure 6; see Supporting Information, Figure S44) that are consistent with molecular C_s symmetry, in line with the crystal structure of this complex. The pyr-H and aldimino proton signals each evolved into two 2H singlets at 213 K, and the α- and β-CH_2 signals similarly resolved into 2H and 1H multiplets.

The accumulated ^{1}H NMR data for **[Cu$_3$Cl(PPh$_3$)$_2$]$^{2+}$** support both a ground state solution-phase geometry no higher than C_s symmetry and the presence of at least three thermally accessible dynamic exchange processes in solution. One involves Lewis base dissociation and is susceptible to the binding strength of the donor. Another involves folding and unfolding of the macrocyclic ligand and appears to be gated by Lewis base dissociation. The latter of these necessitates significant restructuring of the [Cu$_3$Cl]$^{2+}$ core through a process that is not discernable at present. A third process involves the net "rotation" of the intact [Cu$_3$ClL$_2$]$^{2+}$ core within the folded macrocycle, as needed to equilibrate the pyr-H and aldimine protons. This third process may also involve dissociation and reassociation of Cu^+ or CuCl fragments.

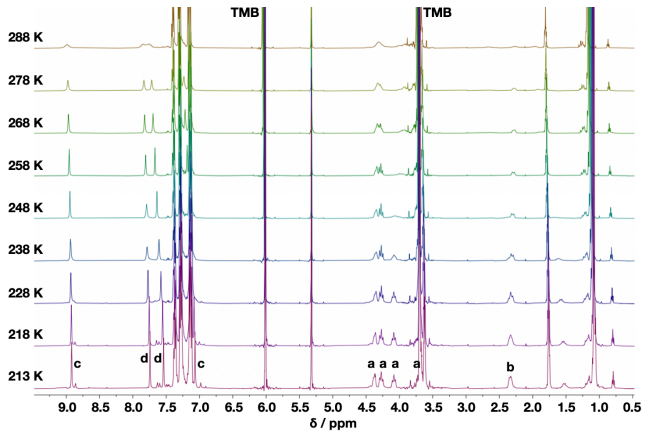

Figure 6. Variable-temperature ^{1}H NMR spectra of **[Cu$_3$Cl(PPh$_3$)$_2$]$^{2+}$** in CD_2Cl_2 in the range of 213 to 298 K. Trimethoxybenzene was added as an internal standard. The α-CH_2 signals are labelled with "a", the β-CH_2 signals are labelled with "b", the aldimino hydrogen signals are labelled with "c", and the pyr-H signals are labelled with "d", The trimethoxybenzene peaks are labelled with "TMB".

Interconversion between Dicopper and Tricopper Complexes

While attempts to perturb a hypothetical equilibrium involving the dissociation of Cu^+ from the tricopper complexes were not fruitful, we did find that a single Cu^+ ion could be removed to generate a new dicuprous cluster. Treatment of a THF solution of **[Cu$_3$Cl(PPh$_3$)$_2$]$^{2+}$** with 1.0 equiv of NaO^{t}Bu resulted in the formation of a red-orange solution after stirring at room temperature for one day. Layering of this solution with *n*-hexane at -35 °C afforded red crystals of **[Cu$_2$Cl(PPh$_3$)$_2$]$^+$**, as determined from single

crystal XRD analysis (Figure 7). The crystallographic metrics of this complex are tabulated in Table 3.

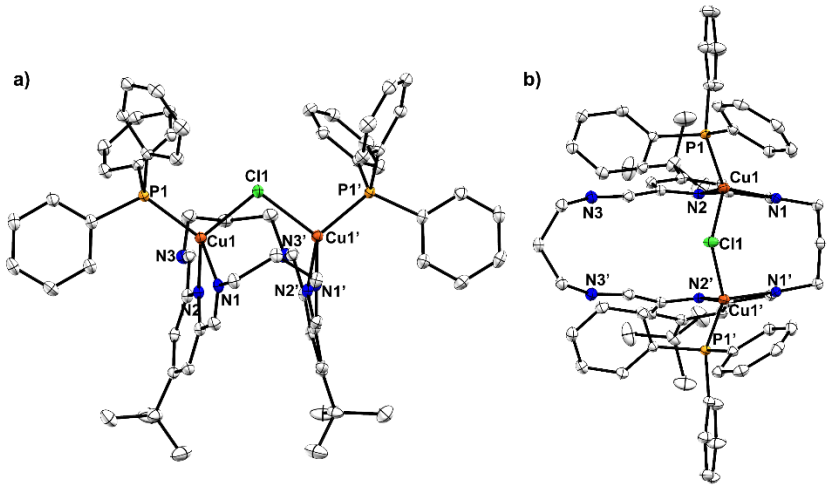

Figure 7. The crystal structure of **[Cu$_2$Cl(PPh$_3$)$_2$]$^+$** with thermal ellipsoids at the probability level of 50%. Hydrogen atoms were omitted for clarity. a) top view; b) side view.

Each Cu center in **[Cu$_2$Cl(PPh$_3$)$_2$]$^+$** is four-coordinate and adopts a distorted tetrahedral geometry (τ_4 = 0.81), involving one PPh$_3$ ligand, the bridging Cl atom, one N_{py} atom, and one N_{ald} atom. The two N_{ald} atoms serving as ligands are connected by a $(CH_2)_3$ linker. The long Cu–Cu distance in **[Cu$_2$Cl(PPh$_3$)$_2$]$^+$** (3.6641(7) Å) and large FSR value (1.56) are indicative of the absence of an attractive interaction between the copper centers.

Table 3. Averaged crystallographic metrics of **[Cu$_2$Cl(PPh$_3$)$_2$]$^+$**.

	[$Cu_2Cl(PPh_3)_2$]$^+$
d(Cu1···Cu1') / Å	3.6641(7)
d(Cu–P) / Å	2.2000(5)
d(Cu–N_{py}) / Å	2.1043(15)
d(Cu–N_{ald}) / Å	2.0578(15)
d(N_{py}-C_{ipso}) / Å	1.349
d(C_{ipso}-C_{ald}) / Å	1.477
d(C_{ald}-N_{ald}) / Å	1.274
Δ_{expt} / Å	0.165
FSR	1.56
τ_4	0.81

The conformation of the neutral ^{3}PDAI$_2$ ligand (Δ = 0.165 Å) in this complex is unusual. The ^{3}PDAI$_2$ ligand adopts a folded conformation similar to those observed in other dicopper and tricopper macrocyclic complexes presented herein. However, the lone pairs on the unbound nitrogen atoms point away from the metal centers in a manner reminiscent of the monocopper and monosilver complexes discussed above. **[$Cu_2Cl(PPh_3)_2$]$^+$** is best described as C_s-symmetric, but NMR spectroscopic studies revealed that this complex exhibits C_{2v}-symmetry in CD_3CN at room temperature, as evidenced by the two low-field 4H singlets, assigned to pyr-H and aldimino H atoms, and the 4:4:2:2 grouping of the multiplets from the $(CH_2)_3$ linkers in its ^{1}H NMR spectrum (see Supporting Information, Figure S12). A likely explanation for this higher solution-phase symmetry on the NMR timescale is a dynamic exchange process that

involves the $[Cu_2Cl(PPh_3)_2]$ core changing position between $[N(CH_2)_3N]$ arms. This would be accompanied by a change in the conformation of the two $[N(CH_2)_3N]$ arms with respect to the orientation of the N_{ald} lone pairs (Scheme 5).

Scheme 5. Proposed dynamic exchange process of **$[Cu_2Cl(PPh_3)_2]^+$** in solution.

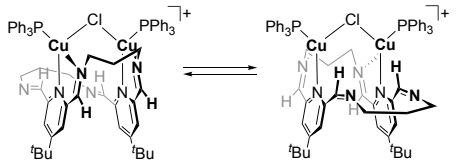

Consistent with this exchange process, the inverted, non-coordinating arm on the $^3PDAI_2$ ligand of **$[Cu_2Cl(PPh_3)_2]^+$** was found to be kinetically competent for rebinding an additional equivalent of Cu^+. The reaction between **$[Cu_2Cl(PPh_3)_2]^+$** and 1.0 equiv. of $[Cu(MeCN)_4][OTf]$ in CD_3CN successfully reformed the tricopper species **$[Cu_3Cl(PPh_3)_2]^{2+}$** (Scheme 6; see Supporting Information, Figure S18). Gratifyingly, this strategy extends to the dicopper complex **$[Cu_2(CNxyl)_2]^{2+}$**. Treatment of a CD_3CN solution of **$[Cu_2(CNxyl)_2]^{2+}$** with 1.0 equiv. of CuCl successfully formed **$[Cu_3Cl(CNxyl)_2]^{2+}$** (see Supporting Information, Figure S11). These results demonstrate the successful control over the interconversion between dicopper and tricopper species by way of Cu atom addition and Cu atom removal (Scheme 6).

Scheme 6. Interconversion between dicopper complexes and tricopper complexes.

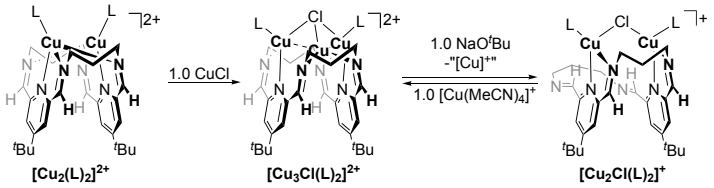

Formation of a Tetracopper Complex

Finally, we discovered that the nuclearity of the copper complexes could be increased further from the trinuclear species described above. Treatment of **[Cu$_3$Cl(NCMe)$_2$]$^{2+}$** in MeCN with 1.0 equiv of CuCl and 4.0 equiv of $NaBPh_4$ resulted in the formation of a dark red solution. Upon work-up and purification, dark red crystals of the tetracopper species [(^{3}PDAI$_2$)Cu$_4$Ph$_2$][BPh$_4$]$_2$ (**[Cu$_4$Ph$_2$]$^{2+}$**) were isolated in a yield of 52 % (Scheme 7). The mechanism of this reaction is unclear, but the stoichiometry of the reaction is consistent with two BPh_4^- ions serving as Ph^- donors to yield **[Cu$_4$Ph$_2$]$^{2+}$**, 2 NaCl, and 2 BPh_3. This reactivity is reminiscent of the aryl group transfer reaction from tetraarylborato anions mediated by the [(DPFN)Cu$_2$(NCMe)]$^{2+}$ complex reported by the Tilley group.[60]

Scheme 7. Synthesis of **[Cu$_4$Ph$_2$]$^{2+}$**.

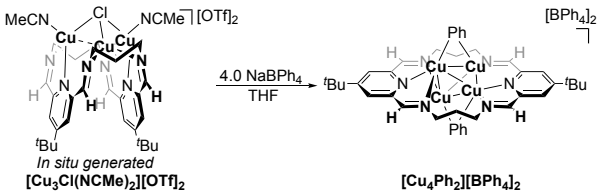

The crystal structure of **[Cu_4Ph_2]$^{2+}$** is depicted in Figure 8. The neutral ^{3}PDAI$_2$ ligand (Δ = 0.160 Å) adopts an unfolded conformation to accommodate the tetracopper core. The four copper atoms form a distorted tetrahedron (Figure 8b). Cu1 and Cu4 are each coordinated to one N_{py} and one N_{ald} connected by a $(CH_2)_3$ linker, while Cu2 and Cu4 are each coordinated to one of the other two N_{ald} atoms. The two μ-Ph groups bridge Cu1-Cu2 and Cu3-C4, respectively, but neither is coordinated symmetrically between the Cu centers, as evidenced by the different Cu–C bond lengths (Table 4). This is different from the binding mode of the μ-Ph and μ-Mes groups to the di-cuprous center in closely related [(DPFN)Cu_2(μ-Ph)]$^+$ [60] and [($^{t\text{-Bu}}$PNNP)Cu_2(μ-Mes)]$^+$ complexes,[54] in which the two Cu–C bond lengths are nearly identical. The Cu2-C29 and Cu3-C35 distances of 1.957(3) and 1.954(4) Å, respectively, in the [Cu_4Ph_2]$^{2+}$ core, are *ca.* 0.05 Å shorter than the Cu1-C29 and Cu4-C35 distances of 2.012(3) and 1.996(4) Å. The symmetry of **[Cu_4Ph_2]$^{2+}$** in the solid state is pseudo-C_2 due to the asymmetric coordination mode of the [Cu_4Ph_2]$^{2+}$ core. However, the ^{1}H NMR spectrum of this complex in CD_3CN shows signals that are consistent with a D_{2h}-symmetric geometry, indicating the presence, again, of multiple dynamic exchange processes in the solution phase. In this case, the absence of neutral Lewis base donors and the unfolded geometry of the ligand in the solid state suggest that dynamic exchange of the ^{3}PDAI$_2$ donors about the [Cu_4Ph_2]$^{2+}$ core likely accounts for the observed solution-phase symmetry.

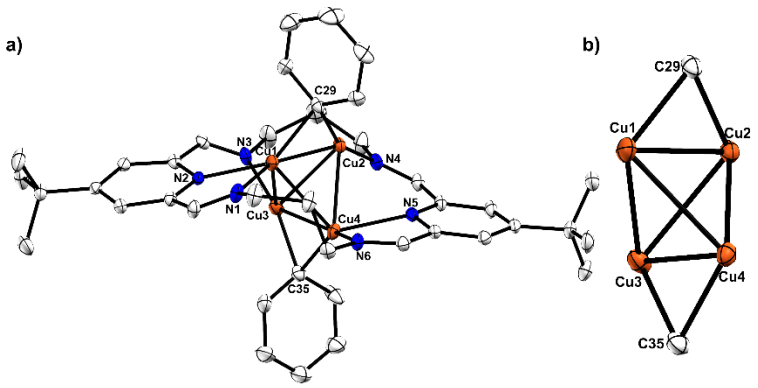

Figure 8. a) Crystal structure of [**Cu**$_4$**Ph**$_2$]$^{2+}$ and b) depiction of the [**Cu**$_4$**Ph**$_2$]$^{2+}$ core within the tetracopper complex with thermal ellipsoids at the probability level of 50%. Hydrogen atoms were omitted for clarity.

Table 4. Averaged crystallographic metrics of [**Cu**$_4$**Ph**$_2$]$^{2+}$.

	[**Cu**$_4$**Ph**$_2$]$^{2+}$
d(Cu1–Cu2) / Å	2.4985(6)
d(Cu1–Cu3) / Å	2.6789(7)
d(Cu1–Cu4) / Å	2.6106(6)
d(Cu2–Cu3) / Å	2.5621(6)
d(Cu2–Cu4) / Å	2.5661(7)
d(Cu3–Cu4) / Å	2.4567(6)
d(Cu1–C29) / Å	2.012(3)
d(Cu2–C29) / Å	1.957(3)
d(Cu3–C35) / Å	1.954(4)
d(Cu4–C35) / Å	1.996(4)
FSR(Cu1–Cu2)	1.07

FSR(Cu1–Cu3)	1.14
FSR(Cu1–Cu4)	1.11
FSR(Cu2–Cu3)	1.09
FSR(Cu2–Cu4)	1.09
FSR(Cu2–Cu5)	1.05

Summary and Conclusions

This work demonstrated the ability to kinetically stabilize the size of Cu(I) clusters contained within a flexible macrocycle through the rational synthesis of mono-, di-, tri-, and tetra-copper systems. The mononuclear and dinuclear Cu(I) complexes **[Cu]**$^{+}$ and **[Cu$_2$(CNxyl)$_2$]**$^{2+}$ were synthesized from the corresponding Ag(I) complexes *via* AgI elimination. Attempts to synthesize a PPh$_3$-coordinated dicuprous complex using this same method serendipitously resulted in the formation of a trinuclear complex, **[Cu$_3$Cl(PPh$_3$)$_2$]**$^{2+}$. A series of isostructural tricopper complexes **[Cu$_3$Cl(L)$_2$]**$^{2+}$ (L = MeCN, xylNC, PMe$_3$ and PPh$_3$) were then synthesized *via* treatment of **[Ag$_2$(NCMe)$_2$]**$^{2+}$ with 3.0 equiv of CuCl in the presence of various Lewis bases (L). The interconversion between trinuclear and dinuclear copper complexes was successfully achieved by way of Cu atom removal (*via* treatment with NaO^{t}Bu), which could then be reversed through Cu atom addition (*via* addition of CuCl or [Cu(MeCN)$_4$]$^{+}$). While all complexes reported in this study exhibit apparent dynamic exchange processes on the NMR timescale in solution at room temperature, the tricopper series was studied in detail due

to the complexity of the dynamic exchange and the ability to perturb the exchange rate through the identity of L. This study revealed the facile exchange of bonds between the ligands and the Cu(I) centers, allowing for loss of ligands L and rapid interconversion of the ^{3}PDAI$_2$-based N–Cu bonding interactions to yield high-symmetries in solution while retaining the number of Cu centers within the cluster. Finally, it was shown that the nuclearity of the system could be further increased by treatment of **[Cu$_3$Cl(L)$_2$]$^{2+}$** with CuCl in the presence of a Ph$^-$ donor, thereby generating the tetracopper species **[Cu$_4$Ph$_2$]$^{2+}$**. This latter system contains a tetrahedral array of Cu(I) ions supported by the ^{3}PDAI$_2$ ligand and two μ^2-Ph ligands. Together, this synthetic study highlights the ability of geometrically flexible, multinucleating ligands to support atomically precise Cu(I) clusters of various sizes to the exclusion of cluster redistribution processes. Efforts to examine the physical properties of these clusters and expand the size of the atomically precise clusters that may be formed through this bottom-up approach are of interest for further study.

Experimental Section

General Considerations

All reactions involving transition metals were performed under an inert atmosphere of dry N_2 in a PureLab HE glovebox or using standard Schlenk techniques unless otherwise noted.

Glassware, stir bars, filter aid (Celite) and 4Å molecular sieves were dried in an oven at 150 °C for at least 12 h prior to use. All solvents (*n*-hexane, diethyl ether, THF, dichloromethane, acetonitrile) were dried by passage through a column of activated alumina, deoxygenated by sparging with N_2 for 15 min, and stored over 4Å molecular sieves unless otherwise noted. Deuterated solvents were purchased from Cambridge Isotope Laboratories, Inc., and dried over either Na/benzophenone (THF-d_8) or CaH_2 (CD_2Cl_2, acetonitrile-d_3) and stored under N_2 over activated 4Å molecular sieves. [(^{3}PDAI$_2$)Ag][BPh$_4$] (**[Ag]$^+$**), [(^{3}PDAI$_2$)Ag(NCMe)][OTf]$_2$ (**[Ag$_2$(NCMe)]$^{2+}$**), [(^{3}PDAI$_2$)Ag(PPh$_3$)$_2$][OTf]$_2$ (**[Ag(PPh$_3$)$_2$]$^{2+}$**) and [(^{3}PDAI$_2$)Ag(CNxyl)$_2$][OTf]$_2$ (**[Ag(CNxyl)$_2$]$^{2+}$**) were synthesized following previously reported procedures.[69] **[Ag$_2$(NCMe)]$^{2+}$** was dried under vacuum (30 mbar) at 40 °C for 6h and stored in a glovebox under dry nitrogen prior to use. $AgNO_3$ (99.9%-Ag), CuCl (anhydrous, 98%), CuI (99.999%-Cu) and NaBPh$_4$ (99.5%+) were purchased from Strem Chemicals and used without further purification. 2,6-dimethylphenyl isocyanide (xylNC) was purchased from Alfa Aesar and used without further purification. NaO^{t}Bu and [Cu(MeCN)$_4$][OTf] were purchased from MilliporeSigma and used without further purification. PMe_3 (98%) was purchased from Strem Chemicals or synthesized according to literature procedures,[89] and was stored as a 1 M solution in THF at -35 °C under dry nitrogen in a glovebox. PPh_3 was purchased from MilliporeSigma, recrystallized from hot ethanol, dried under vacuum (30 mbar) at 40 °C for 6h, and stored in a glovebox under dry nitrogen prior to use.[90] Elemental analyses were performed under an inert atmosphere by Midwest Microlab LLC or at

the University of Rochester (PerkinElmer 2400 Series II). ^{1}H, $^{13}C\{^{1}H\}$, $^{11}B\{^{1}H\}$, $^{31}P\{^{1}H\}$, $^{19}F\{^{1}H\}$, ^{13}C-^{1}H HSQC, ^{13}C-^{1}H HMBC and ^{1}H-^{1}H COSY NMR spectra were recorded on Bruker UNI 400, UNI 500 or NEO 600 spectrometers. All chemical shifts (δ) are reported in units of ppm, with references to the residual protio-solvent resonance for proton and carbon chemical shifts. External $BF_3{\cdot}Et_2O$, H_3PO_4 and $CFCl_3$ were used for referencing ^{31}P and ^{19}F NMR chemical shifts, respectively. No uncommon hazards are noted.

X-ray Crystallography

X-ray intensity data were collected on a Rigaku XtaLAB Synergy-S diffractometer equipped with an HPC area detector (Dectris Pilatus3 R 200K for **[Cu$_2$(CNxyl)$_2$]$^{2+}$**, **[Cu$_2$Cl(PPh$_3$)$_2$]$^{+}$**, **[Cu$_3$Cl(CNxyl)$_2$]$^{2+}$** and **[Cu$_3$Cl(PPh$_3$)$_2$]$^{2+}$** or HyPix-6000HE for **[Cu]$^{+}$**, **[Cu$_3$Cl(PMe$_3$)$_2$]$^{2+}$** and **[Cu$_3$Cl(NCMe)$_2$]$^{2+}$**) or a Bruker APEX II CCD area detector (**[Cu$_4$Ph$_2$]$^{2+}$**) with confocal multilayer optic-monochromated Mo Kα radiation (λ = 0.71073 Å: **[Cu$_2$(CNxyl)$_2$]$^{2+}$**, **[Cu$_3$Cl(CNxyl)$_2$]$^{2+}$**, **[Cu$_3$Cl(PPh$_3$)$_2$]$^{2+}$**, **[Cu$_3$Cl(PMe$_3$)$_2$]$^{+}$** and **[Cu$_3$Cl(NCMe)$_2$]$^{2+}$**), graphite-monochromated Mo Kα radiation (λ = 0.71073 Å: **[Cu$_4$Ph$_2$]$^{2+}$**), or Cu Kα radiation (λ = 1.54184 Å: **[Cu]$^{+}$**) at 100 K. Rotation frames were integrated using CrysAlisPro[91] (**[Cu$_2$(CNxyl)$_2$]$^{2+}$**, **[Cu$_2$Cl(PPh$_3$)$_2$]$^{+}$**, **[Cu$_3$Cl(CNxyl)$_2$]$^{2+}$**, **[Cu$_3$Cl(PPh$_3$)$_2$]$^{2+}$**, **[Cu]$^{+}$**, **[Cu$_3$Cl(PMe$_3$)$_2$]$^{2+}$** and **[Cu$_3$Cl(NCMe)$_2$]$^{2+}$**) or SAINT[92] (**[Cu$_4$Ph$_2$]$^{2+}$**), producing a listing of unaveraged F^2 and $\sigma(F^2)$ values. The intensity data

were corrected for Lorentz and polarization effects and for absorption using SCALE3 ABSPACK[93] (**[Cu$_2$(CNxyl)$_2$]$^{2+}$**, **[Cu$_2$Cl(PPh$_3$)$_2$]$^{+}$**, **[Cu$_3$Cl(CNxyl)$_2$]$^{2+}$**, **[Cu$_3$Cl(PPh$_3$)$_2$]$^{2+}$**, **[Cu]$^{+}$**, **[Cu$_3$Cl(PMe$_3$)$_2$]$^{2+}$** and **[Cu$_3$Cl(NCMe)$_2$]$^{2+}$**) or SADABS[94] (**[Cu$_4$Ph$_2$]$^{2+}$**). The structures were solved by direct methods by using SHELXT[95] and refined by full-matrix least squares, based on F^2 using SHELXL-2018.[95] For **[Cu$_2$(CNxyl)$_2$]$^{2+}$**, the asymmetric unit consists of two macrocycles, two triflate ions and three molecules of THF. In addition, the second molecule displays a large amount of disorder. For **[Cu$_3$Cl(NCMe)$_2$]$^{2+}$**, there was a region of disordered solvent for which a reliable disorder model could not be devised; the X-ray data were corrected for the presence of disordered solvent using SQUEEZE.[96] Crystal parameters and refinement results are given in the Supporting Information, Tables S1-S4.

Syntheses

Synthesis of [(^{3}PDAI$_2$)Cu][BPh$_4$] ([Cu]$^{+}$). CuI (6.8 mg, 0.0357 mmol) was added to a solution of **[Ag]$^{+}$** (32.0 mg, 0.0361 mmol) in THF (6 mL). The resulting purple-red slurry was stirred at room temperature for 2 h then filtered through Celite. The filtrate was layered with 12 mL of *n*-hexane. Storage of the system at room temperature for 2 d yielded **[Cu]$^{+}$** as dark red crystals. Yield: 21.0 mg (64 %). ^{1}H NMR (600 MHz, THF-d_8, 25 °C): δ = 8.30 (s, 4H, C*H*=N), 8.08 (s, 4H, py *m*-H), 7.31 (m, 8H, Ph *o*-*H*), 6.83 (t, 8H, $^3J_{HH}$ = 7.4 Hz, Ph m-*H*), 6.67 (t, 4H, $^3J_{HH}$ = 7.1 Hz, Ph *p*-*H*), 3.71 (br s, 8H, C*H*$_2$CH$_2$C*H*$_2$),

2.14 (br s, 4H, $CH_2CH_2CH_2$), 1.41 (s, 18H, $C(CH_3)_3$) ppm. $^{13}C\{^1H\}$ NMR (151 MHz, THF-d_8, 25 °C): δ = 165.42 (q, $^1J_{BC}$ = 49.3 Hz, BPh_4 *C*), 164.61 (s, py *C*), 162.85 (s, *C*H=N), 153.64 (s, py *C*), 137.38 (br s, BPh_4 *o*-*C*), 126.00 (q, $^3J_{BC}$ = 2.2 Hz, BPh_4 *m*-*C*), 125.10 (s, py *m*-*C*), 122.04 (s, BPh_4 *p*-*C*), 57.45 (s, $CH_2CH_2CH_2$), 36.42 (s, $C(CH_3)_3$), 30.72 (t, *J* = 14.2 Hz, $CH_2CH_2CH_2$) , 30.60 (s, $C(CH_3)_3$) ppm. $^{11}B\{^1H\}$ NMR (128 MHz, THF-d_8, 25 °C): δ = -7.01 (s, *B*Ph_4) ppm. Anal. Calcd. for $C_{56}H_{68}BCuN_6O$ (915.51 g/mol): C, 73.47; H, 7.49; N, 9.18. Found: C, 72.61; H, 6.96; N, 9.13.

Synthesis of [(^{3}PDAI$_2$)Cu$_2$(CNxyl)$_2$][OTf]$_2$ ([Cu$_2$(CNxyl)$_2$]$^{2+}$). CuI (15.9 mg, 0.083 mmol) was added to a solution of **[Ag$_2$(CNxyl)$_2$]$^{2+}$** (50.9 mg, 0.038 mmol) in THF (6 mL). The resulting orange slurry was stirred at room temperature for 1.5 h then filtered through Celite. The filtrate was layered with 12 mL of *n*-hexane. Storage of the system at room temperature for 2 d afforded **[Cu$_2$(CNxyl)$_2$]$^{2+}$** as dark red rods. Yield: 37.4mg (78%). ^1H NMR (500 MHz, CD_2Cl_2, 25 °C): δ = 8.61 (s, 4H, C*H*=N), 7.78 (s, 4H, py *m*-*H*), 7.25 (t, $^3J_{HH}$ = 7.6 Hz, 2H, Ar *p*-*H*), 7.08 (d, $^3J_{HH}$ = 7.6 Hz, 4H, Ar *m*-*H*), 4.45 (br t, $^2J_{HH}$ = 8.0 Hz, 4H, $CH_2CH_2CH_2$), 4.25 (br s, 4H, $CH_2CH_2CH_2$), 2.85 (br s, 2H, $CH_2CH_2CH_2$), 2.42 (br s, 2H, $CH_2CH_2CH_2$), 2.26 (s, 12H, $ArCH_3$), 1.27 (s, 18H, $C(CH_3)_3$) ppm. $^{13}C\{^1H\}$ NMR (126 MHz, CD_2Cl_2, 25 °C): δ = 165.71 (s, py *C*), 162.98 (s, *C*H=N), 151.22 (s, py *C*), 148.67 (br s, N≡*C*), 135.29 (s, Ph *o*-*C*), 130.19 (s, Ph *p*-*C*), 128.64 (s, Ph *m*-*C*), 127.73 (s, py *m*-*C*), 126.37 (br s, CN–*C*), 59.90 (s, $CH_2CH_2CH_2$), 35.88 (s, $C(CH_3)_3$), 34.32 (s, $CH_2CH_2CH_2$), 30.16 (s, $C(CH_3)_3$), 18.81 (s, $ArCH_3$) ppm. Anal. Calcd. for

$C_{54}H_{67.5}Cu_2F_6N_8O_{7.5}S_2$ (1253.89 g/mol): C, 51.73; H, 5.43; N, 8.94. Found: C, 51.46; H, 5.27; N, 9.25.

Synthesis of [(^{3}PDAI$_2$)Cu$_3$(μ_3-Cl)(NCMe)$_2$][OTf]$_2$ ([(Cu$_3$Cl(NCMe)$_2$]$^{2+}$). **[Ag$_2$(NCMe)]$^{2+}$** (50.6 mg, 0.0499 mmol) was dissolved in 6 mL of acetonitrile. The reaction mixture was stirred at room temperature for 5 min, then CuCl (15.1 mg, 0.153 mmol) was added. The slurry immediately turned brown and was stirred at room temperature for 1.5 h. Volatile materials were removed under reduced pressure. Soluble materials were extracted from the solid residue with 6 mL of a 1:1 mixture of THF and MeCN. The resulting mixture was filtered through Celite, and the filtrate was layered with 12 mL of diethyl ether. Storage of the system at room temperature for 7 d afforded **[Cu$_3$Cl(NCMe)$_2$]$^{2+}$** as black blocks. Yield: 16.0 mg (30 %). ^{1}H NMR (600 MHz, CD_3CN, 25 °C): δ = 8.53 (s, 4H, C*H*=N), 7.66 (s, 4H, py *m*-H), 3.95 (t, $^2J_{HH}$ = 4.7 Hz, 8H, C*H*$_2$CH$_2$C*H*$_2$), 2.55 (br s, 4H, CH$_2$C*H*$_2$CH$_2$), 1.21 (s, 18H, C(C*H*$_3$)$_3$) ppm. Coordinated MeCN was not observed, presumably due to exchange with the solvent. ^{13}C{^{1}H} NMR (151 MHz, CD_3CN, 25 °C): δ = 164.06 (s, py *C*), 162.14 (s, *C*H=N), 152.09 (s, py *C*), 123.56 (s, py *m*-C), 122.25 (q, $^1J_{FC}$ = 321.0 Hz, *C*F$_3$SO$_3$), 62.76 (s, *C*H$_2$CH$_2$*C*H$_2$), 35.99 (s, *C*(CH$_3$)$_3$), 30.45 (s, C(*C*H$_3$)$_3$) , 29.36 (s, CH$_2$*C*H$_2$CH$_2$) ppm.^{31}P{^{1}H} NMR (162 MHz, CD_3CN, 25 °C): δ = -3.25 (br s, *P*Ph$_3$) ppm. ^{19}F{^{1}H} NMR (376 MHz, CD_2Cl_2, 30 °C): δ = -79.34 (s, C*F*$_3$SO$_3$) ppm. Anal. Calcd. for $C_{34}H_{44}ClCu_3F_6N_8O_6S_2$ (1064.97 g/mol): C, 38.35; H, 4.16; N, 10.52. Found: C, 38.84; H, 4.15; N, 10.24.

Synthesis of [(^{3}PDAI$_2$)Cu$_3$(μ_3-Cl)(CNxyl)$_2$][OTf]$_2$ ([Cu$_3$Cl(CNxyl)$_2$]$^{2+}$). **[Ag$_2$(NCMe)]$^{2+}$** (46.2 mg, 0.046 mmol) was dispersed in 6 mL of THF, and 2,6-dimethylphenyl isocyanide (12.9 mg, 0.98 mmol) was added as a solid. The reaction mixture turned to a pale golden yellow color in 5 min. CuCl (16.4 mg, 0.166 mmol) was then added as a solid. The resulted dark orange slurry was stirred at room temperature for 45 min and filtered through Celite. The filtrate was layered with 12 mL of *n*-hexane. Storage of the system at room temperature for 3 d yielded **[Cu$_3$Cl(CNxyl)$_2$]$^{2+}$** as red rods. Yield: 38.9 mg (61 %). ^{1}H NMR (600 MHz, CD$_3$CN, 25 °C): δ = 8.60 (s, 4H, C*H*=N), 7.67 (s, 4H, py *m*-H), 7.27 (t, $^3J_{HH}$ = 7.6 Hz, 2H, Ph *p-H*), 7.15 (d, $^3J_{HH}$ = 7.6 Hz, 4H, Ph *m-H*), 4.10 (br t, *J* = 11.0 Hz, 8H, C*H*$_2$CH$_2$C*H*$_2$), 2.61 (br s, 4H, CH$_2$C*H*$_2$CH$_2$), 2.29 (s, 6H, PhC*H*$_3$) 1.22 (s, 18H, C(C*H*$_3$)$_3$) ppm. ^{13}C{^{1}H} NMR (151 MHz, CD$_3$CN, 25 °C): δ = 164.22 (s, py *C*), 162.24 (s, *C*H=N), 152.24 (s, py *C*), 149.77 (br s, *C*≡N), 136.11(s, Ph *o-C*), 130.53 (s, Ph *p-C*), 129.03 (s, Ph *m-C*) , 127.22 (m, CN–*C*), 123.29 (br s, py *m*-C), 122.20 (q, $^1J_{FC}$ = 321.0 Hz, *C*F$_3$SO$_3$), 63.34 (s, *C*H$_2$CH$_2$*C*H$_2$), 36.03 (s, *C*(CH$_3$)$_3$), 30.52 (s, C(*C*H$_3$)$_3$) , 28.88 (s, CH$_2$*C*H$_2$CH$_2$), 18.79 (s, Ph(*C*H$_3$)$_2$) ppm. ^{19}F{^{1}H} NMR (376 MHz, CD$_3$CN, 30 °C): δ = -79.33 (s, C*F*$_3$SO$_3$) ppm. Anal. Calcd. for C$_{48}$H$_{56}$ClCu$_3$F$_6$N$_8$O$_6$S$_2$ (1245.22 g/mol): C, 46.30; H, 4.53; N, 9.00. Found: C, 48.42; H, 4.67; N, 9.12.

Synthesis of [(^{3}PDAI$_2$)Cu$_3$(μ_3-Cl)(PMe$_3$)$_2$][OTf]$_2$ ([Cu$_3$Cl(PMe$_3$)$_2$]$^{2+}$). **[Ag$_2$(NCMe)]$^{2+}$** (51.8 mg, 0.041 mmol) was dispersed in 6 mL of THF, and a solution of PMe$_3$ in THF (1 M, 0.12 mL, 0.12 mmol) was added to the slurry. The reaction mixture immediately turned to a pale golden yellow color. The solution was stirred at room temperature for

10 min, then CuCl (15.7 mg, 0.159 mmol) was added as a solid. The resulting red slurry was stirred at room temperature for 1 h. Volatile materials were removed under vacuum, and soluble materials were extracted from the solid residue with 6 mL of THF. The mixture was filtered through Celite and the filtrate was layered with 12 mL of *n*-hexane. Storage of the system at room temperature for 6 d afforded **[$Cu_3Cl(PMe_3)_2$]$^{2+}$** as black blocks. Yield: 24.5 mg (40 %). ^{1}H NMR (400 MHz, CD_3CN, 25 °C): δ = 8.53 (s, 4H, C*H*=N), 7.63 (s, 4H, py *m*-H), 4.04 (s, 8H, C*H*$_2$CH$_2$C*H*$_2$), 2.69 (br s, 2H, CH$_2$C*H*$_2$CH$_2$), 2.34 (br s, 2H, CH$_2$C*H*$_2$CH$_2$), 1.21 (s, 18H, C(C*H*$_3$)$_3$), 1.09 (br s, 18H, P(C*H*$_3$)$_3$) ppm. ^{13}C{^{1}H} NMR (151 MHz, CD_3CN, 25 °C): δ = 163.67 (s, py *C*), 161.99 (s, *C*H=N), 152.19 (s, py *C*), 123.06 (s, py *m*-C), 122.24 (q, $^1J_{FC}$ = 321.2 Hz, *C*F$_3$SO$_3$), 63.24 (s, *C*H$_2$CH$_2$*C*H$_2$), 35.94 (s, *C*(CH$_3$)$_3$), 30.51 (s, C(*C*H$_3$)$_3$) , 29.06 (br s, CH$_2$*C*H$_2$CH$_2$), 14.93 (d, $^1J_{PC}$ = 20.0 Hz, P(*C*H$_3$)$_3$) ppm. ^{31}P{^{1}H} NMR (162 MHz, CD_3CN, 25 °C): δ = -48.78 (br s, *P*Me$_3$) ppm. Anal. Calcd. for $C_{40}H_{64}ClCu_3F_6N_6O_7P_2S_2$ (1207.13 g/mol): C, 39.80; H, 5.34; N, 6.96. Found: C, 38.88; H, 5.28; N, 6.86.

Synthesis of [(^{3}PDAI$_2$)Cu$_3$(μ_3-Cl)(PPh$_3$)$_2$][OTf]$_2$ ([Cu$_3$Cl(PPh$_3$)$_2$]$^{2+}$). [Ag$_2$(NCMe)]$^{2+}$ (100 mg, 0.0986 mmol) was dispersed in 6 mL of THF, and PPh$_3$ (51.9 mg, 0.198 mmol) was added as a solid. The resulting pale golden yellow solution was stirred at room temperature for 5 min before CuCl (31.5 mg, 0.318 mmol) was added as a solid. The resulting dark orange slurry was stirred at room temperature for 3 h, then filtered through Celite. The filtrate was layered with 12 mL of *n*-hexane. Storage of the system at room temperature for 2 d afforded **[Cu$_3$Cl(PPh$_3$)$_2$]$^{2+}$** as orange needles and black

blocks. The orange needles and black blocks were found to be different polymorphs of the product. Yield: 118.8 mg (79 %). ^{1}H NMR (600 MHz, CD_3CN, 25 °C): δ = 8.46 (s, 4H, C*H*=N), 7.51 (s, 4H, py *m*-H), 7.41 (s, 6H, PPh_3 *p-H*), 7.34 (s, 12H, PPh_3 *m-H*), 7.26 (s, 12H, PPh_3 *o-H*), 3.94 (s, 4H, $CH_2CH_2CH_2$), 3.83 (s, 4H, $CH_2CH_2CH_2$), 2.84 (s, 2H, $CH_2CH_2CH_2$), 2.31 (s, 2H, $CH_2CH_2CH_2$), 1.16 (s, 18H, $C(CH_3)_3$) ppm. ^{13}C{^{1}H} NMR (151 MHz, CD_3CN, 25 °C): δ = 163.76 (s, py *C*), 162.20 (s, *C*H=N), 152.03 (br s, py *C*), 134.25 (br s, P–*C*), 134.00 (d, $^{2}J_{PC}$ = 15.1 Hz, Ph *o-C*), 133.92 (d, $^{2}J_{PC}$ = 15.1 Hz, Ph *o-C*), 131.10 (s, Ph *p-C*), 129.80 (d, $^{3}J_{PC}$ = 9.3 Hz, Ph *m-C*), 122.90 (s, py *m*-C), 122.21 (q, $^{1}J_{FC}$ = 321.1 Hz, *C*F_3SO_3), 63.31 (s, *C*H_2CH_2*C*H_2), 35.92 (s, *C*$(CH_3)_3$), 30.55 (s, C(*C*$H_3)_3$) , 28.41 (s, CH_2*C*H_2CH_2) ppm.^{31}P{^{1}H} NMR (162 MHz, CD_3CN, 25 °C): δ = -3.86 (br s, *P*Ph_3) ppm. ^{19}F{^{1}H} NMR (376 MHz, CD_3CN, 25 °C): δ = -79.32 (s, C*F*$_3SO_3$) ppm. Anal. Calcd. for $C_{66}H_{68}ClCu_3F_6N_6O_6P_2S_2$ (1507.45 g/mol): C, 52.59; H, 4.55; N, 5.58. Found: C, 52.35; H, 4.39; N, 5.47.

Synthesis of [(^{3}PDAI$_2$)Cu$_2$(μ-Cl)(PPh$_3$)$_2$][OTf] ([Cu$_2$Cl(PPh$_3$)$_2$]$^{+}$). **[Cu$_3$Cl(PPh$_3$)$_2$]$^{2+}$** (27.1 mg, 0.0179 mmol) was dissolved in THF, followed by the addition of NaO^{t}Bu (1.9 mg, 0.020 mmol) as a solid. The mixture was stirred at room temperature for 30 h, then filtered through Celite. The orange filtrate was layered with 12 mL of *n*-hexane. Storage of the system at -35 °C for 5 d yielded **[Cu$_2$Cl(PPh$_3$)$_2$]$^{+}$** as red rods. Yield: 16.5 mg (64 %). ^{1}H NMR (600 MHz, CD_3CN, 25 °C): δ = 8.46 (s, 4H, C*H*=N), 7.48 (s, 4H, py *m*-H), 7.39 (m, 6H, PPh_3 *p-H*), 7.32 (m, 12H, PPh_3 *m-H*), 7.23 (m, 12H, PPh_3 *o-H*), 3.95 (t, $^{2}J_{HH}$ = 10.4 Hz, 4H, $CH_2CH_2CH_2$), 3.79 (t, $^{2}J_{HH}$ = 8.8 Hz, 4H, $CH_2CH_2CH_2$), 2.85 (br s, 2H,

$CH_2CH_2CH_2$), 2.31 (m, 2H, $CH_2CH_2CH_2$), 1.16 (s, 18H, $C(CH_3)_3$) ppm. $^{13}C\{^1H\}$ NMR (151 MHz, CD_3CN, 25 °C): δ = 163.68 (s, py *C*), 162.19 (s, *C*H=N), 152.04 (br s, py *C*), 134.31 (d, $^1J_{PC}$ = 30.0 Hz, P–*C*), 133.92 (d, $^2J_{PC}$ = 15.1 Hz, Ph *o*-*C*), 131.00 (d, $^4J_{PC}$ = 1.0 Hz, Ph *p*-*C*), 129.75 (d, $^3J_{PC}$ = 9.3 Hz, Ph *m*-*C*), 122.82 (s, py *m*-C), 63.75 (s, $CH_2CH_2CH_2$), 35.91 (s, $C(CH_3)_3$), 30.57 (s, $C(CH_3)_3$) , 28.20 (s, $CH_2CH_2CH_2$) ppm.$^{31}P\{^1H\}$ NMR (162 MHz, CD_3CN, 25 °C): δ = -3.25 (br s, *P*Ph_3) ppm. $^{19}F\{^1H\}$ NMR (376 MHz, CD_2Cl_2, 30 °C): δ = -79.35 (s, CF_3SO_3) ppm. Anal. Calcd. for $C_{65}H_{68}ClCu_2F_3N_6O_3P_2S$ (1294.84 g/mol): C, 60.29; H, 5.29; N, 6.49. Found: C, 56.28; H, 4.85; N, 6.04.

Synthesis of $[(^3PDAI_2)Cu_4(\mu\text{-}Ph)_2][BPh_4]_2$ ($[Cu_4Ph_2]^{2+}$). $[Ag_2(NCMe)]^{2+}$ (49.6 mg, 0.049 mmol) was dissolved in acetonitrile and stirred at room temperature for 5 min. CuCl (21.0 mg, 0.212 mmol) was added as a solid. The reaction mixture immediately turned brown. After 5 min, $NaBPh_4$ (69.4 mg, 0.203 mmol) was added to the slurry as a solid. The reaction mixture was stirred at room temperature for 2 d, then filtered through Celite. All volatile materials were removed under reduced pressure, and soluble materials were extracted from the solid residue with 6 mL of THF. The resulting mixture was filtered through Celite, and the filtrate was layered with 12 mL of *n*-hexane. Storage of the system at room temperature for 9 d afforded $[Cu_4Ph_2]^{2+}$ as dark red needles. Yield: 46.9 mg (52%). There are two disordered molecules of $[Cu_4Ph_2]^{2+}$ in one asymmetric unit of the crystal. Alternatively $[Cu_4Ph_2]^{2+}$ was crystallized by storing a solution of the complex in MeCN layered under Et_2O at room temperature. The crystals obtained from this latter method contain one molecule of $[Cu_4Ph_2]^{2+}$ that is free

from disorder in one asymmetric unit. The two crystals were found to contain identical complexes by ^{1}H NMR spectroscopic studies. The parameters and metrics of **[Cu$_4$Ph$_2$]$^{2+}$** are thus reported using the non-disordered crystal structure. ^{1}H NMR (500 MHz, CD_3CN, 25 °C): δ = 8.62 (s, 4H, C*H*=N), 7.76 (br s, 4H, py *m-H* and br s, 2H μ-Ph *o-H*), 7.27 (m, 16H, BPh_4 *m-H*), 7.20 (t, $^{3}J_{HH}$ = 7.7 Hz, 2H, μ-Ph *p-H*), 7.10 (t, 4H, $^{3}J_{HH}$ = 8.5 Hz, μ-Ph *m-H*), 6.99 (t, $^{3}J_{HH}$ =7.1 Hz, 16H, BPh_4 *o-H*), 6.83 (t, $^{3}J_{HH}$ =6.7 Hz, 8H, BPh_4 *p*-H), 4.09 (s, 8H, $CH_2CH_2CH_2$), 2.56 (br s, 4H, $CH_2CH_2CH_2$), 1.26 (s, 18H, $C(CH_3)_3$) ppm. Signals for the *o*-H of the μ-Ph groups could not be located. ^{13}C{^{1}H} NMR (CD_3CN, 126 MHz, 25 °C) δ = 164.78 (q, $^{1}J_{BC}$ = 49.3 Hz, B–*C*), 163.21 (br s), 151.94 (s), 145.28 (s), 136.70 (q, $^{3}J_{BC}$ = 1.2 Hz, BPh_4 *m-C*), 129.30 (s), 127.89 (s, μ-Ph *m-C*), 126.59 (q, $^{2}J_{BC}$ = 2.8 Hz, BPh_4 *o-C*), 122.75 (s, BPh_4 *p-C*), 62.50 (s, $CH_2CH_2CH_2$), 36.14 (s, $C(CH_3)_3$), 30.36 (s, $C(CH_3)_3$), 30.18 (m, $CH_2CH_2CH_2$) ppm. Signals for three of the carbons are missing; these may correspond to the ipso carbons on the pyridyl and μ-Ph rings. ^{11}B{^{1}H} NMR (CD_3CN, 80.6 MHz, 25 °C): δ = -7.12 (s, *B*Ph_4) ppm. Anal. Calcd. for $C_{106.25}H_{124.75}B_2Cu_4N_6O_{4.375}$ (1831.64 g/mol): C, 69.67; H, 6.86; N, 4.59. Found: C, 67.71; H, 6.19; N, 5.59.

ASSOCIATED CONTENT

Supporting Information

The Supporting Information is available free of charge on the ACS Publications website.

NMR spectra, crystallographic details, tabulated bond metrics (PDF)

Accession Codes

CCDC 2360559-2360566 contain the supplementary crystallographic data for this paper. These data can be obtained free of charge via www.ccdc.cam.ac.uk/data_request/cif, by emailing data_request@ccdc.cam.ac.uk, or by contacting The Cambridge Crystallographic Data Centre, 12 Union Road, Cambridge CB2 1EZ, U.K.; Fax: + 44 1223 336033.

AUTHOR INFORMATION

Corresponding Author

* E-mail: tomson@upenn.edu; Phone: +1-215-898-6208

ACKNOWLEDGMENT

We thank the National Science Foundation's Division of Chemistry (CHE-1945265) and the National Institute of General Medical Sciences of the National Institutes of Health (R35GM128794) for financial support.

REFERENCES

(1) Friedfeld, M. R.; Stein, J. L.; Cossairt, B. M. Main-Group-Semiconductor Cluster Molecules as Synthetic Intermediates to Nanostructures. *Inorg. Chem.* **2017**, *56* (15), 8689-8697. DOI: 10.1021/acs.inorgchem.7b00291

(2) Wu, Z.; Tallu, M.; Stuhrmann, G.; Dehnen, S. Ligand-functionalized and ligand-bridged or organyl-separated chalcogenido metalate-based clusters. *Coord. Chem. Rev.* **2023**, *497*, 215424. DOI: 10.1016/j.ccr.2023.215424

(3) Kanady, J. S.; Tsui, E. Y.; Day, M. W.; Agapie, T. A Synthetic Model of the Mn_3Ca Subsite of the Oxygen-Evolving Complex in Photosystem II. *Science* **2011**, *333* (6043), 733-736. DOI: 10.1126/science.1206036

(4) Ye, M.; Thompson, N. B.; Brown, A. C.; Suess, D. L. M. A Synthetic Model of Enzymatic $[Fe_4S_4]$–Alkyl Intermediates. *J. Am. Chem. Soc.* **2019**, *141* (34), 13330-13335. DOI: 10.1021/jacs.9b06975

(5) Schilter, D.; Camara, J. M.; Huynh, M. T.; Hammes-Schiffer, S.; Rauchfuss, T. B. Hydrogenase Enzymes and Their Synthetic Models: The Role of Metal Hydrides. *Chem. Rev.* **2016**, *116* (15), 8693-8749. DOI: 10.1021/acs.chemrev.6b00180

(6) Di Francesco, G. N.; Gaillard, A.; Ghiviriga, I.; Abboud, K. A.; Murray, L. J. Modeling Biological Copper Clusters: Synthesis of a Tricopper Complex, and Its Chloride- and Sulfide-Bridged Congeners. *Inorg. Chem.* **2014**, *53* (9), 4647-4654. DOI: 10.1021/ic500333p

(7) Friedle, S.; Reisner, E.; Lippard, S. J. Current challenges of modeling diiron enzyme active sites for dioxygen activation by biomimetic synthetic complexes. *Chem. Soc. Rev.* **2010**, *39* (8), 2768-2779. DOI: 10.1039/C003079C

(8) Liu, T.; Gau, M. R.; Tomson, N. C. Mimicking the Constrained Geometry of a Nitrogen-Fixation Intermediate. *J. Am. Chem. Soc.* **2020**, *142* (18), 8142-8146. DOI: 10.1021/jacs.0c01861

(9) Sekretaryova, A.; Jones, S. M.; Solomon, E. I. O_2 Reduction to Water by High Potential Multicopper Oxidases: Contributions of the T1 Copper Site Potential and the Local Environment of the Trinuclear Copper Cluster. *J. Am. Chem. Soc.* **2019**, *141* (28), 11304-11314. DOI: 10.1021/jacs.9b05230

(10) Bergmann, L.; Braun, C.; Nieger, M.; Bräse, S. The coordination- and photochemistry of copper(I) complexes: variation of N^N ligands from imidazole to tetrazole. *Dalton Trans.* **2018**, *47* (2), 608-621. DOI: 10.1039/C7DT03682E

(11) Ke, F.; Song, Y.; Li, H.; Zhou, C.; Du, Y.; Zhu, M. Sub-nanometer Cu(I) clusters: coordination-modulated (Se vs. S) atom-packing mode and emission. *Dalton Trans.* **2019**, *48* (37), 13921-13924. DOI: 10.1039/C9DT02908G

(12) Gennari, M.; Lanfranchi, M.; Cammi, R.; Pellinghelli, M. A.; Marchiò, L. Mononuclear and Polynuclear Copper(I) Complexes with a New N,N',S-Donor Ligand and with Structural

Analogies to the Copper Thionein Core. *Inorg. Chem.* **2007**, *46* (24), 10143-10152. DOI: 10.1021/ic701189b

(13) Li, H.; Zhai, H.; Zhou, C.; Song, Y.; Ke, F.; Xu, W. W.; Zhu, M. Atomically Precise Copper Cluster with Intensely Near-Infrared Luminescence and Its Mechanism. *J. Phys. Chem. Lett.* **2020**, *11* (12), 4891-4896. DOI: 10.1021/acs.jpclett.0c01358

(14) Li, Y.-L.; Wang, Z.-Y.; Ma, X.-H.; Luo, P.; Du, C.-X.; Zang, S.-Q. Distinct photophysical properties in atom-precise silver and copper nanocluster analogues. *Nanoscale* **2019**, *11* (12), 5151-5157. DOI: 10.1039/C9NR01058K

(15) Xiang, J.; Cheng, S.-C.; Jin, X.-X.; Su, Q.-Q.; Zhou, X.; Chu, W.-K.; Leung, C.-F.; Ko, C.-C. Polynuclear Cu(I) and Ag(I) phosphine complexes containing multi-dentate polytopic ligands: syntheses, crystal structures and photoluminescence properties. *Dalton Trans.* **2019**, *48* (2), 741-750. DOI: 10.1039/C8DT03377C

(16) Sun, C.; Mammen, N.; Kaappa, S.; Yuan, P.; Deng, G.; Zhao, C.; Yan, J.; Malola, S.; Honkala, K.; Häkkinen, H.; Teo, B. K.; Zheng, N. Atomically Precise, Thiolated Copper–Hydride Nanoclusters as Single-Site Hydrogenation Catalysts for Ketones in Mild Conditions. *ACS Nano* **2019**, *13* (5), 5975-5986. DOI: 10.1021/acsnano.9b02052

(17) Deutsch, C.; Krause, N.; Lipshutz, B. H. CuH-Catalyzed Reactions. *Chem. Rev.* **2008**, *108* (8), 2916-2927. DOI: 10.1021/cr0684321

(18) Schmid, R.; Broger, E. A.; Cereghetti, M.; Crameri, Y.; Foricher, J.; Lalonde, M.; Müller, R. K.; Scalone, M.; Schoettel, G.; Zutter, U. New developments in enantioselective hydrogenation. **1996**, *68* (1), 131-138. DOI: doi:10.1351/pac199668010131

(19) Saito, T.; Yokozawa, T.; Ishizaki, T.; Moroi, T.; Sayo, N.; Miura, T.; Kumobayashi, H. New Chiral Diphosphine Ligands Designed to have a Narrow Dihedral Angle in the Biaryl Backbone. *Adv. Synth. Catal.* **2001**, *343* (3), 264-267. DOI: 10.1002/1615-4169(20010330)343:3<264::AID-ADSC264>3.0.CO;2-T

(20) Blaser, H.-U.; Brieden, W.; Pugin, B.; Spindler, F.; Studer, M.; Togni, A. Solvias Josiphos Ligands: From Discovery to Technical Applications. *Top. Catal.* **2002**, *19* (1), 3-16. DOI: 10.1023/A:1013832630565

(21) Sass, D. C.; de Lucca, E. C.; da Silva Barbosa, J.; de Oliveira, K. T.; Constantino, M. G. Tandem reduction + cyclization of ortho-substituted cinnamic esters. *Tet. Lett.* **2011**, *52* (41), 5371-5374. DOI: 10.1016/j.tetlet.2011.08.039

(22) Sass, D. C.; Gomes Heleno, V. C.; Callegari Lopes, J. L.; Constantino, M. G. One-step biomimetic conversion of a furanoheliangolide into an eremantholide using Stryker's reagent. *Tet. Lett.* **2008**, *49* (24), 3877-3880. DOI: 10.1016/j.tetlet.2008.04.071

(23) Singh, K.; Long, J. R.; Stavropoulos, P. Polynuclear Complexes of Copper(I) and the 2-(3(5)-Pyrazolyl)-6-methylpyridine Ligand: Structures and Reactivity toward Small Molecules. *Inorg. Chem.* **1998**, *37* (5), 1073-1079. DOI: 10.1021/ic9708071

(24) Ziegler, M. S.; Lakshmi, K. V.; Tilley, T. D. Dicopper Cu(I)Cu(I) and Cu(I)Cu(II) Complexes in Copper-Catalyzed Azide–Alkyne Cycloaddition. *J. Am. Chem. Soc.* **2017**, *139* (15), 5378-5386. DOI: 10.1021/jacs.6b13261

(25) Cook, B. J.; Di Francesco, G. N.; Ferreira, R. B.; Lukens, J. T.; Silberstein, K. E.; Keegan, B. C.; Catalano, V. J.; Lancaster, K. M.; Shearer, J.; Murray, L. J. Chalcogen Impact on Covalency within Molecular $[Cu_3(\mu_3\text{-}E)]^{3+}$ Clusters (E = O, S, Se): A Synthetic, Spectroscopic, and Computational Study. *Inorg. Chem.* **2018**, *57* (18), 11382-11392. DOI: 10.1021/acs.inorgchem.8b01000

(26) Kounalis, E.; Lutz, M.; Broere, D. L. J. Cooperative H_2 Activation on Dicopper(I) Facilitated by Reversible Dearomatization of an "Expanded PNNP Pincer" Ligand. *Chem. Eur. J.* **2019**, *25* (58), 13280-13284. DOI: 10.1002/chem.201903724

(27) Hermann, H. L.; Boche, G.; Schwerdtfeger, P. Metallophilic Interactions in Closed-Shell Copper(I) Compounds—A Theoretical Study. *Chem. Eur. J.* **2001**, *7* (24), 5333-5342. DOI: 10.1002/1521-3765(20011217)7:24<5333::AID-CHEM5333>3.0.CO;2-1

(28) Raju, S.; Singh, H. B.; Butcher, R. J. Metallophilic interactions: observations of the shortest metallophilicinteractions between closed shell ($d^{10}\cdots d^{10}$, $d^{10}\cdots d^{8}$, $d^{8}\cdots d^{8}$) metal ions [M···M′ M = Hg(II) and Pd(II) and M′ = Cu(I), Ag(I), Au(I), and Pd(II)]. *Dalton Trans.* **2020**, *49* (26), 9099-9117. DOI: 10.1039/D0DT01008A

(29) Harisomayajula, N. V. S.; Makovetskyi, S.; Tsai, Y.-C. Cuprophilic Interactions in and between Molecular Entities. *Chem. Eur. J.* **2019**, *25* (38), 8936-8954. DOI: 10.1002/chem.201900332

(30) Gray, T. G.; Sadighi, J. P. Group 11 Metal–Metal Bonds. In *Molecular Metal - Metal Bonds*, **2015**; pp 397-428.

(31) Wallesch, M.; Volz, D.; Zink, D. M.; Schepers, U.; Nieger, M.; Baumann, T.; Bräse, S. Bright Coppertunities: Multinuclear CuI Complexes with N–P Ligands and Their Applications. *Chem. Eur. J.* **2014**, *20* (22), 6578-6590. DOI: 10.1002/chem.201402060

(32) Desnoyer, A. N.; Nicolay, A.; Ziegler, M. S.; Torquato, N. A.; Tilley, T. D. A Dicopper Platform that Stabilizes the Formation of Pentanuclear Coinage Metal Hydride Complexes. *Angew. Chem. Int. Ed.* **2020**, *59* (31), 12769-12773. DOI: 10.1002/anie.202004346

(33) Lane, A. C.; Vollmer, M. V.; Laber, C. H.; Melgarejo, D. Y.; Chiarella, G. M.; Fackler, J. P., Jr.; Yang, X.; Baker, G. A.; Walensky, J. R. Multinuclear Copper(I) and Silver(I) Amidinate Complexes: Synthesis, Luminescence, and CS_2 Insertion Reactivity. *Inorg. Chem.* **2014**, *53* (21), 11357-11366. DOI: 10.1021/ic501694d

(34) Plotzitzka, J.; Kleeberg, C. [(NHC)Cu^{I}–ER_3] Complexes (ER_3 = $SiMe_2Ph$, $SiPh_3$, $SnMe_3$): From Linear, Mononuclear Complexes to Polynuclear Complexes with Ultrashort Cu^{I}···Cu^{I} Distances. *Inorg. Chem.* **2016**, *55* (10), 4813-4823. DOI: 10.1021/acs.inorgchem.6b00210

(35) Filatov, A. S.; Hietsoi, O.; Sevryugina, Y.; Gerasimchuk, N. N.; Petrukhina, M. A. Reversible Cu_4 ↔ Cu_6 Core Interconversion and Temperature Induced Single-Crystal-to-Single-Crystal Phase Transition for Copper(I) Carboxylate. *Inorg. Chem.* **2010**, *49* (4), 1626-1633. DOI: 10.1021/ic9020367

(36) Liu, C.-Y.; Yuan, S.-F.; Wang, S.; Guan, Z.-J.; Jiang, D.-e.; Wang, Q.-M. Structural transformation and catalytic hydrogenation activity of amidinate-protected copper hydride clusters. *Nat. Commun.* **2022**, *13* (1), 2082. DOI: 10.1038/s41467-022-29819-y

(37) Kleeberg, C.; Borner, C. Syntheses, Structures, and Reactivity of NHC Copper(I) Boryl Complexes: A Systematic Study. *Organometallics* **2018**, *37* (21), 4136-4146. DOI: 10.1021/acs.organomet.8b00672

(38) Fernandes, G. F. S.; Machado, F. B. C.; Ferrão, L. F. A. Identification of Magic Numbers in Homonuclear Clusters: The ε^3 Stability Ranking Function. *J. Phys. Chem. A* **2020**, *124* (2), 454-463. DOI: 10.1021/acs.jpca.9b11264

(39) Ge, X.; Zeng, S.; Deng, H.; Teo, B. K.; Sun, C. Atom-precise copper nanoclusters based on FCC, BCC, and HCP structures. *Coord. Chem. Rev.* **2024**, *503*, 215667. DOI: 10.1016/j.ccr.2024.215667

(40) Li, C.-G.; Shen, Z.-G.; Hu, Y.-F.; Tang, Y.-N.; Chen, W.-G.; Ren, B.-Z. Insights into the structures and electronic properties of Cu_{n+1}^{μ} and Cu_nS^{μ} ($n = 1–12$; $\mu = 0, \pm1$) clusters. *Sci. Rep.* **2017**, *7* (1), 1345. DOI: 10.1038/s41598-017-01444-6

(41) Chang, X.-Y.; Low, K.-H.; Wang, J.-Y.; Huang, J.-S.; Che, C.-M. From Cluster to Polymer: Ligand Cone Angle Controlled Syntheses and Structures of Copper(I) Alkynyl Complexes. *Angew. Chem. Int. Ed.* **2016**, *55* (35), 10312-10316. DOI: 10.1002/anie.201604762

(42) Dhayal, R. S.; van Zyl, W. E.; Liu, C. W. Polyhydrido Copper Clusters: Synthetic Advances, Structural Diversity, and Nanocluster-to-Nanoparticle Conversion. *Acc. Chem. Res.* **2016**, *49* (1), 86-95. DOI: 10.1021/acs.accounts.5b00375

(43) Edwards, A. J.; Dhayal, R. S.; Liao, P.-K.; Liao, J.-H.; Chiang, M.-H.; Piltz, R. O.; Kahlal, S.; Saillard, J.-Y.; Liu, C. W. Chinese Puzzle Molecule: A 15 Hydride, 28 Copper Atom Nanoball. *Angew. Chem. Int. Ed.* **2014**, *53* (28), 7214-7218. DOI: 10.1002/anie.201403324

(44) Shimada, K.; Kobayashi, A.; Ono, Y.; Ohara, H.; Hasegawa, T.; Taketsugu, T.; Sakuda, E.; Akagi, S.; Kitamura, N.; Kato, M. Core-Structure-Dependent Luminescence of Thiolato-Bridged Copper(I) Cluster Complexes. *J. Phys. Chem. C* **2016**, *120* (29), 16002-16011. DOI: 10.1021/acs.jpcc.5b12688

(45) Xu, C.; Yi, X.-Y.; Duan, T.-K.; Chen, Q.; Zhang, Q.-F. Thiolate-bridged polynuclear clusters of copper(I) and silver(I): Syntheses and structures of $[Cu_8(\mu_4\text{-}SPh)_6(PPh_3)_4(MeCN)_4][(CdI)_3Cu(\mu\text{-}SPh)_6]$, $[Cu_8(\mu\text{-}SPh)_4(\mu_3\text{-}SPh)_4(PPh_3)_4]$, $[Cu_{14}(\mu_6\text{-}S)(\mu_3\text{-}SPhMe\text{-}4)_{12}(PPh_3)_6]$, and $[Ag_{14}(\mu_6\text{-}Br)(\mu_3\text{-}SPh)_{12}(PPh_3)_8]Cl$. *Polyhedron* **2011**, *30* (16), 2637-2643. DOI: 10.1016/j.poly.2011.06.023

(46) Yuan, P.; Chen, R.; Zhang, X.; Chen, F.; Yan, J.; Sun, C.; Ou, D.; Peng, J.; Lin, S.; Tang, Z.; Teo, B. K.; Zheng, L.-S.; Zheng, N. Ether-Soluble Cu_{53} Nanoclusters as an Effective Precursor of High-Quality CuI Films for Optoelectronic Applications. *Angew. Chem. Int. Ed.* **2019**, *58* (3), 835-839. DOI: 10.1002/anie.201812236

(47) Zhang, M.-M.; Dong, X.-Y.; Wang, Z.-Y.; Li, H.-Y.; Li, S.-J.; Zhao, X.; Zang, S.-Q. AIE Triggers the Circularly Polarized Luminescence of Atomically Precise Enantiomeric Copper(I) Alkynyl Clusters. *Angew. Chem. Int. Ed.* **2020**, *59* (25), 10052-10058. DOI: 10.1002/anie.201908909

(48) Zhuo, H.-Y.; Su, H.-F.; Cao, Z.-Z.; Liu, W.; Wang, S.-A.; Feng, L.; Zhuang, G.-L.; Lin, S.-C.; Kurmoo, M.; Tung, C.-H.; Sun, D.; Zheng, L.-S. High-Nuclear Organometallic Copper(I)–Alkynide Clusters: Thermochromic Near-Infrared Luminescence and Solution Stability. *Chem. Eur. J.* **2016**, *22* (49), 17619-17626. DOI: 10.1002/chem.201603797

(49) Davenport, T. C.; Tilley, T. D. Dinucleating Naphthyridine-Based Ligand for Assembly of Bridged Dicopper(I) Centers: Three-Center Two-Electron Bonding Involving an Acetonitrile Donor. *Angew. Chem. Int. Ed.* **2011**, *50* (51), 12205-12208. DOI: 10.1002/anie.201106081

(50) Tsui, E. Y.; Day, M. W.; Agapie, T. Trinucleating Copper: Synthesis and Magnetostructural Characterization of Complexes Supported by a Hexapyridyl 1,3,5-

Triarylbenzene Ligand. *Angew. Chem. Int. Ed.* **2011**, *50* (7), 1668-1672. DOI: 10.1002/anie.201005232

(51) Wang, Q.; Brooks, S. H.; Liu, T.; Tomson, N. C. Tuning metal–metal interactions for cooperative small molecule activation. *Chem. Commun.* **2021**, *57* (23), 2839-2853. DOI: 10.1039/D0CC07721F

(52) van Langevelde, P. H.; Kounalis, E.; Killian, L.; Monkcom, E. C.; Broere, D. L. J.; Hetterscheid, D. G. H. Mechanistic Investigations into the Selective Reduction of Oxygen by a Multicopper Oxidase T3 Site-Inspired Dicopper Complex. *ACS Catal.* **2023**, *13* (8), 5712-5722. DOI: 10.1021/acscatal.3c01143

(53) Bienenmann, R. L. M.; Schanz, A. J.; Ooms, P. L.; Lutz, M.; Broere, D. L. J. A Well-Defined Anionic Dicopper(I) Monohydride Complex that Reacts like a Cluster. *Angew. Chem. Int. Ed.* **2022**, *61* (29), e202202318. DOI: 10.1002/anie.202202318

(54) Kounalis, E.; Lutz, M.; Broere, D. L. J. Tuning the Bonding of a μ-Mesityl Ligand on Dicopper(I) through a Proton-Responsive Expanded PNNP Pincer Ligand. *Organometallics* **2020**, *39* (4), 585-592. DOI: 10.1021/acs.organomet.9b00829

(55) Piesch, M.; Nicolay, A.; Haimerl, M.; Seidl, M.; Balázs, G.; Don Tilley, T.; Scheer, M. Binding, Release and Functionalization of Intact Pnictogen Tetrahedra Coordinated to Dicopper Complexes. *Chem. Eur. J.* **2022**, *28* (45), e202201144. DOI: 10.1002/chem.202201144

(56) Ríos, P.; See, M. S.; Handford, R. C.; Teat, S. J.; Tilley, T. D. Robust dicopper(I) μ-boryl complexes supported by a dinucleating naphthyridine-based ligand. *Chem. Sci.* **2022**, *13* (22), 6619-6625. DOI: 10.1039/D2SC00848C

(57) Nicolay, A.; Héron, J.; Shin, C.; Kuramarohit, S.; Ziegler, M. S.; Balcells, D.; Tilley, T. D. Unsymmetrical Naphthyridine-Based Dicopper(I) Complexes: Synthesis, Stability, and Carbon–Hydrogen Bond Activations. *Organometallics* **2021**, *40* (12), 1866-1873. DOI: 10.1021/acs.organomet.1c00188

(58) Desnoyer, A. N.; Nicolay, A.; Ziegler, M. S.; Lakshmi, K. V.; Cundari, T. R.; Tilley, T. D. A Dicopper Nitrenoid by Oxidation of a CuICuI Core: Synthesis, Electronic Structure, and Reactivity. *J. Am. Chem. Soc.* **2021**, *143* (18), 7135-7143. DOI: 10.1021/jacs.1c02235

(59) Desnoyer, A. N.; Nicolay, A.; Rios, P.; Ziegler, M. S.; Tilley, T. D. Bimetallics in a Nutshell: Complexes Supported by Chelating Naphthyridine-Based Ligands. *Acc. Chem. Res.* **2020**, *53* (9), 1944-1956. DOI: 10.1021/acs.accounts.0c00382

(60) Ziegler, M. S.; Levine, D. S.; Lakshmi, K. V.; Tilley, T. D. Aryl Group Transfer from Tetraarylborato Anions to an Electrophilic Dicopper(I) Center and Mixed-Valence μ-Aryl Dicopper(I,II) Complexes. *J. Am. Chem. Soc.* **2016**, *138* (20), 6484-6491. DOI: 10.1021/jacs.6b00802

(61) Wang, Q.; Zhang, S.; Cui, P.; Weberg, A. B.; Thierer, L. M.; Manor, B. C.; Gau, M. R.; Carroll, P. J.; Tomson, N. C. Interdependent Metal–Metal Bonding and Ligand Redox-Activity

in a Series of Dinuclear Macrocyclic Complexes of Iron, Cobalt, and Nickel. *Inorg. Chem.* **2020**, *59* (7), 4200-4214. DOI: 10.1021/acs.inorgchem.9b02339

(62) Thierer, L. M.; Brooks, S. H.; Weberg, A. B.; Cui, P.; Zhang, S.; Gau, M. R.; Manor, B. C.; Carroll, P. J.; Tomson, N. C. Macrocycle-Induced Modulation of Internuclear Interactions in Homobimetallic Complexes. *Inorg. Chem.* **2022**, *61* (16), 6263-6280. DOI: 10.1021/acs.inorgchem.2c00522

(63) Zhang, S.; Wang, Q.; Thierer, L. M.; Weberg, A. B.; Gau, M. R.; Carroll, P. J.; Tomson, N. C. Tuning Metal–Metal Interactions through Reversible Ligand Folding in a Series of Dinuclear Iron Complexes. *Inorg. Chem.* **2019**, *58* (18), 12234-12244. DOI: 10.1021/acs.inorgchem.9b01673

(64) Zhang, S.; Cui, P.; Liu, T.; Wang, Q.; Longo, T. J.; Thierer, L. M.; Manor, B. C.; Gau, M. R.; Carroll, P. J.; Papaefthymiou, G. C.; Tomson, N. C. N—H Bond Formation at a Diiron Bridging Nitride. *Angew. Chem. Int. Ed.* **2020**, *59* (35), 15215-15219. DOI: 10.1002/anie.202006391

(65) Liu, T.; Murphy, R. P.; Carroll, P. J.; Gau, M. R.; Tomson, N. C. C–C σ-Bond Oxidative Addition and Hydrofunctionalization by a Macrocycle-Supported Diiron Complex. *J. Am. Chem. Soc.* **2022**, *144* (31), 14037-14041. DOI: 10.1021/jacs.2c06266

(66) Cui, P.; Wang, Q.; McCollom, S. P.; Manor, B. C.; Carroll, P. J.; Tomson, N. C. Ring-Size-Modulated Reactivity of Putative Dicobalt-Bridging Nitrides: C—H Activation versus

Phosphinimide Formation. *Angew. Chem. Int. Ed.* **2017**, *56* (50), 15979-15983. DOI: 10.1002/anie.201708966

(67) Spentzos, A. Z.; Gau, M. R.; Carroll, P. J.; Tomson, N. C. Unusual cyanide and methyl binding modes at a dicobalt macrocycle following acetonitrile C–C bond activation. *Chem. Commun.* **2020**, *56* (67), 9675-9678. DOI: 10.1039/D0CC03521A

(68) Brooks, S. H.; Richards, C. A.; Carroll, P. J.; Gau, M. R.; Tomson, N. C. Anion Capture at the Open Core of a Geometrically Flexible Dicopper(II,II) Macrocycle Complex. In *Inorganics*, **2023**; Vol. *11*.

(69) Wang, Q.; Gau, M. R.; Manor, B. C.; Carroll, P. J.; Tomson, N. C. Metallophilic and Inter-Ligand Interactions in Diargentous Compounds Bound by a Geometrically Flexible Macrocycle. *Eur. J. Inorg. Chem.* **2023**, *26* (27), e202300335. DOI: 10.1002/ejic.202300335

(70) Pauling, L. Atomic Radii and Interatomic Distances in Metals. *J. Am. Chem. Soc.* **1947**, *69* (3), 542-553. DOI: 10.1021/ja01195a024

(71) Yang, L.; Powell, D. R.; Houser, R. P. Structural variation in copper(I) complexes with pyridylmethylamide ligands: structural analysis with a new four-coordinate geometry index, τ^4. *Dalton Trans.* **2007**, (9), 955-964. DOI: 10.1039/B617136B

(72) Römelt, C.; Weyhermüller, T.; Wieghardt, K. Structural characteristics of redox-active pyridine-1,6-diimine complexes: Electronic structures and ligand oxidation levels. *Coord. Chem. Rev.* **2019**, *380*, 287-317. DOI: 10.1016/j.ccr.2018.09.018

(73) Thierer, L. M.; Wang, Q.; Brooks, S. H.; Cui, P.; Qi, J.; Gau, M. R.; Manor, B. C.; Carroll, P. J.; Tomson, N. C. Pyridyldiimine macrocyclic ligands: Influences of template ion, linker length and imine substitution on ligand synthesis, structure and redox properties. *Polyhedron* **2021**, *198*, 115044. DOI: 10.1016/j.poly.2021.115044

(74) Bondi, A. van der Waals Volumes and Radii. *J. Phys. Chem.* **1964**, *68* (3), 441-451. DOI: 10.1021/j100785a001

(75) Cotton, F. A. Discovering and understanding multiple metal-to-metal bonds. *Acc. Chem. Res.* **1978**, *11* (6), 225-232. DOI: 10.1021/ar50126a001

(76) Groom, C. R.; Bruno, I. J.; Lightfoot, M. P.; Ward, S. C. The Cambridge Structural Database. *Acta Cryst. B* **2016**, *72* (2), 171-179. DOI: doi:10.1107/S2052520616003954

(77) Cuesta, R.; Ruiz, J.; Moreno, J. M.; Colacio, E. Synthesis and crystal structure of the μ_2-{tris[bis(diphenylphosphine)methane]}-μ_3-3-methyl-8- ethylxanthine-N,O,O]-μ_3-chloro-triangle-tricopper(I)-water complex exhibiting a novel oxopurine coordination mode. *Inorg. Chim. Acta* **1994**, *227* (1), 43-47. DOI: 10.1016/0020-1693(94)04135-0

(78) Kathewad, N.; Pal, S.; Kumawat, R. L.; Ehesan Ali, M.; Khan, S. Synthetic Diversity and Luminescence Properties of $ArN(PPh_2)_2$-Based Copper(I) Complexes. *Eur. J. Inorg. Chem.* **2018**, *2018* (22), 2518-2523. DOI: 10.1002/ejic.201800096

(79) Liaw, B.-J.; Lobana, T. S.; Lin, Y.-W.; Wang, J.-C.; Liu, C. W. Versatility of Dithiophosphates in the Syntheses of Copper(I) Complexes with

Bis(diphenylphosphino)alkanes: Abstraction of Chloride from Dichloromethane. *Inorg. Chem.* **2005**, *44* (26), 9921-9929. DOI: 10.1021/ic051166+

(80) Kodera, M.; Tachi, Y.; Kita, T.; Kobushi, H.; Sumi, Y.; Kano, K.; Shiro, M.; Koikawa, M.; Tokii, T.; Ohba, M.; Okawa, H. A Cu(II)-Mediated C—H Oxygenation of Sterically Hindered Tripyridine Ligands To Form Triangular $Cu(II)_3$ Complexes. *Inorg. Chem.* **2000**, *39* (2), 226-234. DOI: 10.1021/ic990331g

(81) Collins, L. R.; Lowe, J. P.; Mahon, M. F.; Poulten, R. C.; Whittlesey, M. K. Copper Diamidocarbene Complexes: Characterization of Monomeric to Tetrameric Species. *Inorg. Chem.* **2014**, *53* (5), 2699-2707. DOI: 10.1021/ic4031014

(82) Fedorchuk, A. A.; Slyvka, Y. I.; Goreshnik, E. A.; Kityk, I. V.; Czaja, P.; Mys'kiv, M. G. Crystal structure and NLO properties of the novel tetranuclear copper(I) chloride π-complex with 3-allyl-2-(allylimino)-1,3-thiazolidin-4-one. *J. Mol. Struct.* **2018**, *1171*, 644-649. DOI: 10.1016/j.molstruc.2018.06.017

(83) Yang, X.-Y.; Li, Y.; Pullarkat, S. A. A One-Pot Diastereoselective Self Assembly of C-Stereogenic Copper(I) Diphosphine Clusters. *Inorg. Chem.* **2014**, *53* (19), 10232-10239. DOI: 10.1021/ic501233w

(84) Rathnayaka, S. C.; Hsu, C.-W.; Johnson, B. J.; Iniguez, S. J.; Mankad, N. P. Impact of Electronic and Steric Changes of Ligands on the Assembly, Stability, and Redox Activity of

$Cu_4(\mu_4\text{-}S)$ Model Compounds of the CuZ Active Site of Nitrous Oxide Reductase (N_2OR). *Inorg. Chem.* **2020**, *59* (9), 6496-6507. DOI: 10.1021/acs.inorgchem.0c00564

(85) Chen, K.; Shearer, J.; Catalano, V. J. Subtle Modulation of $Cu_4X_4L_2$ Phosphine Cluster Cores Leads to Changes in Luminescence. *Inorg. Chem.* **2015**, *54* (13), 6245-6256. DOI: 10.1021/acs.inorgchem.5b00443

(86) Köhn, R. D.; Pan, Z.; Mahon, M. F.; Kociok-Köhn, G. Trimethyltriazacyclohexane as bridging ligand for triangular Cu_3 units and C–H hydride abstraction into a Cu_6 cluster. *Chem. Commun.* **2003**, (11), 1272-1273. DOI: 10.1039/B302670A

(87) Mukhopadhyay, S.; Mandal, D.; Chatterjee, P. B.; Desplanches, C.; Sutter, J.-P.; Butcher, R. J.; Chaudhury, M. Bi- and Trinuclear Copper(II) Complexes of a Sterically Constrained Phenol-Based Tetradentate Ligand: Syntheses, Structures, and Magnetic Studies. *Inorg. Chem.* **2004**, *43* (26), 8501-8509. DOI: 10.1021/ic049271r

(88) Heppner, D. E.; Kjaergaard, C. H.; Solomon, E. I. Mechanism of the Reduction of the Native Intermediate in the Multicopper Oxidases: Insights into Rapid Intramolecular Electron Transfer in Turnover. *J. Am. Chem. Soc.* **2014**, *136* (51), 17788-17801. DOI: 10.1021/ja509150j

(89) Luetkens Jr., M. L.; Sattelberger, A. P.; Murray, H. H.; Basil, J. D.; Fackler Jr., J. P.; Jones, R. A.; Heaton, D. E. Trimethylphosphine. In *Inorganic Syntheses*, **1989**; pp 7-12.

(90) Armarego, W. L. F.; Chai, C. *Purification of organic chemicals*; Butterworth-Heinemann, **2009**.

(91) *CrysAlisPro*; Rigaku Oxford Diffraction, Rigaku Corporation: Oxford, UK, **2020**.

(92) SAINT v8.38A: Bruker-AXS Madison, Wisconsin, USA. **2014**.

(93) *SCALE3 ABSPACK: an Oxford Diffraction program*; Oxford Diffraction Ltd.: Abingdon, UK, **2005**.

(94) Krause, L.; Herbst-Irmer, R.; Sheldrick, G. M.; Stalke, D. Comparison of silver and molybdenum microfocus X-ray sources for single-crystal structure determination. *J. Appl. Crystallogr.* **2015**, *48* (1), 3-10. DOI: 10.1107/S1600576714022985

(95) Sheldrick, G. SHELXT - Integrated space-group and crystal-structure determination. *Acta Cryst. A* **2015**, *71* (1), 3-8. DOI: doi:10.1107/S2053273314026370

(96) Spek, A. Structure validation in chemical crystallography. *Acta Cryst. D* **2009**, *65* (2), 148-155. DOI: doi:10.1107/S090744490804362X

TOC Graphic

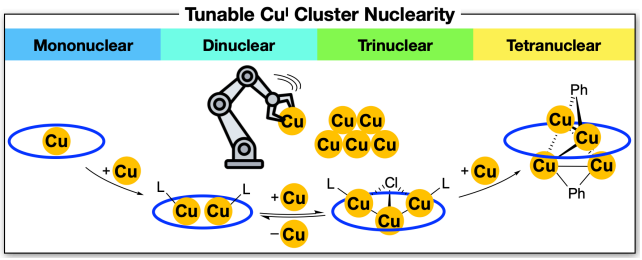

The use of a geometrically flexible multinucleating ligand is used to support the rational syntheses of mono-, di-, tri-, and tetra-cuprous complexes. NMR spectroscopic studies revealed that dynamic solution-phase behavior resulted from ligand exchange and intramolecular rearrangement processes. The interconversion of certain di- and tri-nuclear complexes, as well as the isolation of species with nuclearities ranging from 1-4, supported the notion that the systems are stabilized against redistribution of Cu(I) ions by the macrocyclic framework.